C. R. Palevol 15 (2016) 142–162

Contents lists available at ScienceDirect

Comptes Rendus Palevol

www.sciencedirect.com

General Palaeontology, Systematics and Evolution (Vertebrate Palaeontology)

Bone histology, microanatomy, and growth of the nothosauroid *Simosaurus gaillardoti* (Sauropterygia) from the Upper Muschelkalk of southern Germany/Baden-Württemberg

Histologie, microanatomie et croissance osseuses chez le nothosauridé Simosaurus gaillardoti *(Sauropterygia) du Muschelkalk supérieur d'Allemagne orientale/Bade-Wurtemberg*

Nicole Klein [a,*], Eva Maria Griebeler [b]

[a] *State Museum of Natural History Stuttgart, Rosenstein 1, 70191 Stuttgart, Germany*
[b] *Department of Ecology, Zoological Institute, University of Mainz, 55128 Mainz, Germany*

ARTICLE INFO

Article history:
Received 27 October 2014
Accepted after revision 7 February 2015
Available online 28 August 2015

Handled by Michel Laurin

Keywords:
Coarse parallel-fibred bone
Growth models
Growth rates
Life history data

ABSTRACT

Simosaurus gaillardoti was a large eosauropterygian (Sauropterygia), a group of diverse diapsid marine reptiles. Its occurrence correlates to transgression phases in the Germanic Basin and a former morphological study hypothesized that *Simosaurus* was capable of sustained swimming. Microanatomical analysis of five long bones revealed functional differences between the humerus and femur but did not confirm sustained swimming in *Simosaurus*. It had certain active swimming abilities but – based on microanatomy – it was a less efficient swimmer when compared to contemporaneously living nothosaurs. *Simosaurus* grew with well-vascularized coarse parallel-fibred bone tissue. Growth marks appear as broad zones and thin annuli. Two specimens show an external fundamental system in their outer cortex. For three samples the logistic growth model best describes growth in *Simosaurus*. The estimated ages at death range between 7 and 13 years, asymptotic masses range between 113 and 129 kg and were reached after 10 up to 20 years. Maximum growth rates were between 44 and 69 g per day, and higher than of an extant similar-sized reptile such as *Varanus komodoensis*, *Alligator mississippiensis*, and *Caretta caretta*, but are still consistent with the variability seen in extant reptiles. Growth of one femur followed the von Bertalanffy model but the model's biological reliability is questionable due to an unrealistic high hatchling mass.

Mots clés :
Os grossier à fibres parallèles
Modèles de croissance
Taux de croissance
Données sur l'histoire de vie

RÉSUMÉ

Simosaurus gaillardoti était un grand éosauroptérygien (Sauropterygia), groupe de divers reptiles marins diapsidés. Son occurrence se corrèle avec les phases de transgression dans le Bassin germanique, et une étude morphologique antérieure a permis de formuler l'hypothèse que *Simosaurus* pouvait nager de façon prolongée. L'analyse microanatomique

* Corresponding author.
E-mail address: nicole.klein@smns-bw.de (N. Klein).

http://dx.doi.org/10.1016/j.crpv.2015.02.009
1631-0683/

de cinq os longs révèle des différences fonctionnelles entre l'humérus et le fémur, mais ne confirme pas une capacité de nage prolongée chez *Simosaurus*. Ce dernier a certaines capacités de nage active, mais, sur la base de la microanatomie, c'est un nageur moins efficace que les nothosaures vivant à la même époque. *Simosaurus* grandit avec un tissu osseux grossier à fibres parallèles, bien vascularisé. Les marques de croissance apparaissent sous forme de larges zones ou de minces annuli. Deux spécimens présentent un système fondamental externe dans leur cortex extérieur. Pour trois échantillons, le modèle logistique de croissance décrit au mieux la croissance chez *Simosaurus*. Les âges de mort estimés sont compris entre 7 et 13 ans, les masses asymptotiques sont comprises entre 113 et 129 kg et sont atteintes au bout de 10 à 20 ans. Les taux de croissance maximaux sont de 44 à 69 g par jour, plus élevés que chez des reptiles de même taille, tels *Varanus komodoensis*, *Alligator mississippiensis* et *Caretta caretta*, mais sont encore compatibles avec la variabilité observée chez les reptiles vivants. La croissance de l'un des fémurs suit le modèle de von Bertalanffy, mais la fiabilité biologique du modèle pose question, en raison d'une masse à l'éclosion importante et non réaliste.

1. Introduction

Simosaurus gaillardoti Meyer, 1842 was a member of the marine reptile group Sauropterygia that ranged from the late Early Triassic to the end of the Cretaceous. The Triassic radiation included predominately shallow marine forms such as Placodontia, Pachypleurosauria, Nothosauria, as well as open sea Pistosauria; conversely, the Jurassic and Cretaceous seas were ruled by the open sea Plesiosauria. The latter had a global distribution, whereas most Triassic representatives were largely restricted to the epicontinental seas of the Tethys. *Simosaurus* is a monospecific genus and the sister taxon of all other Eusauropterygia (*Nothosaurus, Lariosaurus, Cymatosaurus, Pistosaurus*) (Chen et al., 2014; Neenan et al., 2013; Rieppel, 1994, 2000). It had a mainly western Tethyan distribution and was stratigraphically restricted to the Middle up to the lower Upper Triassic (Rieppel, 2000). It occurred in the Upper Muschelkalk and Lower Keuper (Ladinian, Middle Triassic) of Luneville (eastern France), Württemberg and Franconia (SW Germany) (Rieppel, 1994). Fragmentary material is described from the Austrian Alps, Israel, and Saudi Arabia (Rieppel, 2000). *Simosaurus* was relatively large with a body length of 3 to 4 meters (Rieppel, 1994). Morphological most characteristic is its brevirostrine, blunt and flattened skull with short and broad lateral teeth. The animals probably used these teeth for crushing of moderately hard-shelled organisms such as "holostean"- fishes and, perhaps, ammonites (Rieppel, 1994:1). However, its slender and delicate lower jaw contradicts a "true" durophageous habit (Rieppel, 1994). Its body was dorsoventrally flattened. The humerus was slender, when compared to other eusauropterygians. Humerus length/distal width ratios could indicate sexual dimorphism in *Simosaurus* (Rieppel, 1994) that was also observed in some pachypleurosaurs (Cheng et al., 2009; Lin and Rieppel, 1998; Sander, 1989). Based on vertebrae morphology, in particular the interlocking of zygapophyses, Rieppel (1994:35) suggested that *Simosaurus* was most likely swimming by paraxial propulsion rather than by lateral undulation. However, *Simosaurus* has slender stylopodial elements when compared to other Eusauropterygia (own obs.) that might contradict a swimming style by paraxial propulsion. Based on morphology Rieppel (1994) suggests that *Simosaurus* was capable of sustained swimming. A complete morphological description of *Simosaurus* is found in Rieppel (1994, 2000).

Bone histological studies reveal insights into bone tissues and growth rates, and thus into metabolism and physiology of extinct taxa (e.g., Bakker, 1980; Montes et al., 2007; Padian and Horner, 2004; Padian et al., 2004; Ricqlès, 1983, 1992). From the preserved growth record, growth patterns and life history strategies can be deduced (e.g., Buffrénil and Castanet, 2000; Castanet et al., 1993; Chinsamy Turan, 2011; Griebeler et al., 2013; Hugi and Sánchez-Villagra, 2012; Klein et al., 2015a, 2015b; Köhler et al., 2012; Sanchez et al., 2010; Sander and Klein, 2005). Bone microstructure (i.e., bone compactness, presence and size of the medullary cavity, presence of a perimedullary region, trabecular organization, vascularity, etc.) has shown to reflect the lifestyle of organisms (e.g., Canoville and Laurin, 2010; Dumont et al., 2013; Houssaye et al., 2010, 2014; Quemeneur et al., 2013). It can also indicate ecological preferences of organisms (e.g., Buffrénil et al., 1987, 1990; Germain and Laurin, 2005; Hayashi et al., 2013; Houssaye et al., 2013; Klein et al., 2015a, 2015b; Laurin et al., 2004, 2007, 2011). Morphology and notably bone histology of Triassic Sauropterygia document a high variety of ecologies including feeding strategies and life histories. These differences enabled them to live contemporaneously in the same habitats (Buffrénil and Mazin, 1992; Houssaye, 2013; Hugi, 2011; Hugi et al., 2011; Klein, 2010; Klein et al., 2015a, 2015b; Krahl et al., 2013; Rieppel, 2000; Sander, 1990).

Two humeri and three femora were sampled to describe long bone histology, growth, and microanatomy of *Simosaurus gaillardoti* and to compare it with that of other Sauropterygia. Different mathematical growth models are applied to four samples that show a well preserved growth record and that originate from different individuals of *Simosaurus gaillardoti*. The statistically best-supported growth curves of different individuals reveal life history characteristics and help to assess life history data of this taxon.

1.1. Modelling of growth and testing of hypotheses

In extant and fossil species, different mathematical sigmoidal growth models have been applied to test and generalize life history characteristics, such as growth rates and ages at important changes during an individual's life (age at death, age at which maximum mass/size is reached, age at sexual maturity; Griebeler et al., 2013; Klein et al., 2015b). Such models are established from the histological growth record preserved in long bones. To find the statistically best supported growth curve out of a set of candidate curves generated Griebeler et al. (2013) developed an objective method that also solves the problem that an unknown number of growth marks could be missing in the inner part of the bone due to resorption and remodeling of inner growth marks. These authors fitted different standard growth models to a growth series preserved in a sauropod long bone. They next checked for the biological plausibility and absolute goodness of fit of raw data to the different candidate models. Finally, they used an Akaike Information Criterion (AIC, Akaike, 1973; Burnham and Anderson, 2002) based model selection process to identify the statistically best out of the biologically reasonable candidate models. The mathematic formulations of standard growth functions reproduce a sigmoidal growth of body mass, and assume that the individual's growth rate, initial and final mass/size are positive numbers. While the residuals of a fitted model provide a good measure of *absolute* goodness of fit of raw data to a non-linear function (Quinn and Keough, 2002), an AIC value is a measure of the *relative* goodness of fit of raw data to a statistical model. A model with a lower AIC value is statistically supported over another having a higher AIC value (Burnham and Anderson, 2002). Therefore, Burnham and Anderson (2002) suggest to calculate ΔAIC scores for each of the candidate models (AIC-min(AIC)) using the model with the lowest AIC as reference (min(AIC)). ΔAIC scores less than two indicate equally well-supported models, scores between 2 and 10 suggest moderate support, and a score >10 indicates a weakly supported model relative to the alternative model (with the lowest AIC, Burnham and Anderson, 2002). Akaike weights are more intuitive than ΔAIC scores on which they are based. Akaike weights can be interpreted as the probability that a model is the best, given the raw data and the set of candidate models tested (Burnham and Anderson, 2002).

The standard growth models applied to growth records of specimens basically differ in the position of the inflection point, which is assumed to coincide with sexual maturation in amphibians and reptiles (e.g., Kupfer et al., 2004; Lee and Werning, 2008; Reiss, 1989; Ritz et al., 2010). The inflection point is at 30% of asymptotic mass under the von Bertalanffy growth model, at 37% of asymptotic mass under the Gompertz model, and at 50% of the asymptotic mass under the logistic growth model (summarized in Fitzhugh, 1976). Under the Chapman-Richards growth model its position is not *a priori* fixed, but it is parametrized in the model equation (Richards, 1959). Thus, contrary to the above mentioned sigmoidal growth models, the Chapman-Richards model is able to generate any sigmoidal growth curve within the two extremes, a monotonic concave increase (no inflection point, maximum growth rate at birth) and a monotonic convex increase (no inflection point, truncated exponential model). Asymptotic mass (length) is defined as the body mass (length) at which the individual is fully grown. After the individual reaches this mass (length), growth severely decreases and essentially stops (= asymptotic phase of growth). Growth models can further reveal ages when asymptotic mass (length) was reached, in the case that the individual died before it reached asymptotic mass (length), and also ages at death, when the growth record is incomplete due to remodeling or resorption of the inner part of the bone. They also provide more accurate estimates of maximum growth rates of individuals than the direct analysis of the histological growth record of a specimen.

2. Material and methods

A complete list of the material included in this study is given in Table 1. The studied bones of *Simosaurus gaillardoti* (Fig. 1) were collected from different bone beds from the Upper Muschelkalk of southern Germany/Baden-Württemberg (Villingen-Schwenningen, Lobenhausen near the river Jagst/Hohenlohe, Stuttgart-Zuffenhausen, quarry Heldenmühle by Crailsheim). They are all stored in the collection of the Stuttgart State Museum of Natural History, Germany (SMNS). Bones were sampled at the midshaft by cutting an entire cross section. Due to preservation in two of the five specimens (SMNS 52095, SMNS 91983, Table 1), the sampling location is distal to the midshaft, and thus not exactly located at midshaft. Midshaft regions of humeri and femora are usually best suited for obtaining the most complete growth record due to the appositional cortical growth (Konietzko-Meier and Klein, 2013; but see Nakajima et al., 2014 for turtles). Additionally, they provide a reasonable proxy for body mass (Anderson et al., 1985). Histological samples were produced following standard petrographic methods (e.g., Klein and Sander, 2007). Thin sections were then studied with a Leica® DMLP compound polarizing microscope, equipped with a digital camera, a Leica® DFC 420C and a Leica® DM 750P compound polarizing microscope equipped with a digital Leica® ICC50HD camera. Cross-sections were scanned with an Epson V740 PRO high-resolution scanner. The bone histological terminology follows Francillon-Vieillot et al. (1990). Bone compactness of the entire cross section was analyzed with the software Bone Profiler (Girondot and Laurin, 2003) (Table 1). Microanatomical values of *Simosaurus* obtained from Bone Profiler were evaluated based on a principal component analysis (PCA). This PCA was conducted for various other Sauropterygia and includes other extinct and extant marine vertebrates. The results of the PCA were recently published by Klein et al. (2015a: figure 8). Bone compactness of the cortex (medulla excluded) was measured with a pixel counting computer program (©P. Göddertz, StIPB), which measures the ratio between vascular spaces and compact bone (Table 1). In the scanned cross sections annual growth cycles were marked by arrows in Adobe Photoshop CS5.1 (Fig. 6). Before they were digitally marked growth marks

Table 1
List of sampled bones of *Simosaurus gaillardoti* and summary of bone histological data derived from the growth record and from growth curve modelling (Table 2). All bones were collected from the Upper Muschelkalk of southern Germany/Baden-Württemberg. Age at death represents the number of completed annual growth cycles.
Tableau 1
Liste des os de *Simosaurus gaillardoti* échantillonnés et données d'histologie des os à partir du registre de croissance et de la modélisation de courbes de croissance (Tableau 2). Tous les os ont été récoltés dans le Muschelkalk supérieur d'Allemagne méridionale, Bade-Wurtemberg. L'âge de la mort représente le nombre de cycles de croissance annuels complets.

Bone spec. no.	bl	p	Sampling location	Body mass at death (kg)	bc%	bc% without medulla	gm	Recon. gm	Age at death (years)	Age at death from gc (years)	Asymptotic age from gc (years)	Onset sm. (years)	Onset sm. from gc (years)	MGR from gc (g per day)
Humerus SMNS 52095	31.5	12.2	Distal	126.3	74.6	90	10 (EFS)	2–3	12–13	10–13	10–13	?	3–4 up to 6–7	64–69
Humerus SMNS 18698	~21	7.7	Midshaft	84.3	81.4	89.5	7	0	7	7	16	?2	5–6	56
Femur SMNS 18689	21.9	7.3	Midshaft	113.5	73	96.5	10	3	13	12	20	?	8–9	44
Femur SMNS 91983	~21.5	7.5	Distal	111.2	83.3	95.4	5	2–4	7–9	No model	No model	?	No model	No model
Femur SMNS 18038	14.2	4.6	Midshaft	73.4	88.5	94.9	7 (EFS)	1	8	7	20	?3-4	1–2	36

bc%: bone compactness in percentage; bl: bone length; EFS: external fundamental system; gc: growth curve (see Table 2); gm: number of growth marks; MGR: maximum growth rate; p: perimeter; Recon. gm: number of reconstructed (missing) growth marks; sm: sexual maturity; ?: unknown or only a rough estimate.

Fig. 1. (Color online.) Photographs of sampled humeri and femora of *Simosaurus gaillardoti* from the Upper Muschelkalk of southern Germany. A. Humerus SMNS 52095 in ventral view. B. Humerus SMNS 18698 in ventral view. C. Distal part of femur SMNS 91983 in ventral view. D. Femur SMNS 18689 in dorsal view. E. Femur SMNS 18038 in dorsal view. Bones were photographed before sampling. The arrows mark the sampling location.
Fig. 1. (Couleur en ligne.) Photographie d'humérus et de fémurs de *Simosaurus gaillardoti* échantillonnés dans le Muschelkalk supérieur d'Allemagne méridionale. A. Humérus SMNS 52095 en vue ventrale. B. Humérus SMNS 18698 en vue ventrale. C. Parie distale du fémur SMNS 91983 en vue ventrale. D. Fémur SMNS 18689 en vue dorsale. E. Fémur SMNS 18038 en vue dorsale. Les os ont été photographiés avant l'échantillonnage. Les flèches indiquent la localisation de l'échantillonnage.

were always double-checked in the original thin section under normal and polarized light.

For estimating the number of annual growth cycles lost in the inner part of a sample, the distance between the centre of the medulla and the first visible annual growth cycle was measured. This distance was then divided by the largest distance observed between two adjacent annual growth cycles that delimit the largest growth cycle of the sample. This method assumes that cycle distances are larger in juvenile than in older individuals (Griebeler et al., 2013; Klein and Sander, 2007).

2.1. Mass reconstruction

Growth curves describe the change in body mass during ontogeny and are based on the histological growth record of the individual. The body mass of the individual is thus needed to establish its growth curve. The body mass at death of each individual was calculated using the equation for standard quadrupeds from Anderson et al. (1985). This equation estimates body mass from the circumference of the humerus and femur of the same individual. It is expected to reveal robust estimates of body mass in

mammalian and non-avian reptilian taxa (Campione and Evans, 2012). Its applicability is untested for secondarily marine vertebrates, which are not standard quadrupeds due to, e.g., differences in body shape and gravity. However, body mass of the semiaquatic *Alligator mississippiensis* was tested in the study of Campione and Evans (2012), which has a dorsoventrally flat and anteroposteriorly elongated body form that is also seen in *Simosaurus*. Body mass calculations for *Simosaurus* are based on the most complete individual SMNS 14733. The specific equation that was used to estimate body mass (W) is

$W = 0.078 \times (7.9 + 6.1)^{2.73}$ [Anderson et al., 1985]

It revealed 105 kg for SMNS 14733. The humerus length of SMNS 14733 is 262 mm, which is 76.5% of the length of the largest humerus known of *Simosaurus* (SMNS 17590; 342 mm). From the humeral length (262 mm) and the body mass (105 kg) of SMNS 14733 the body mass of the sampled individuals (M) was estimated from the length of the humeri (humerus length) applying the equation

M = 105 × humerus length/262.

For the femora SMNS 18038 and SMNS 18698 the corresponding humeral length was estimated assuming a humerus/femur length ratio of 1.29 in *Simosaurus* (Rieppel, 1994; own calculations). The femur length for the distal femur fragment SMNS 91983 (Table 1) was reconstructed from a regression line ($R^2 = 0.8776$) on femur length against distal width (data taken from Rieppel, 1994: Table 6). Resulting body masses are given in Table 1 for each individual.

2.2. Mathematical growth models

To construct a mass-based growth curve for a single individual, the relationship between local bone apposition rate and body mass gain is taken into account. Minimal shaft circumference increases proportionally with bone length and the local bone apposition rate is closely tied to body mass gain. Thus, each growth mark laid down during ontogeny is linked to a respective body mass of the individual. First, to reconstruct respective body masses for growth marks an estimate of the body mass of the individual at death is needed as a reference (Table 1). Next, for each growth mark its distance from the center of the section is measured, and the proportion of this distance and the distance between the center of the section and the outer bone surface of the section is calculated. Then, for each of the growth marks the respective proportions are multiplied by the bone length at death yielding an estimate of the respective bone lengths for each growth mark. Finally, to estimate masses from bone length at each growth mark the equation given in Erickson and Tumanova (2000) was applied.

Mass (bone length) = (bone length^3/bone length at death^3) × body mass at death

The non-linear model fitting procedure used to establish growth curves for specimens is introduced and described in detail in Griebeler et al. (2013). Growth curves for four out of the five *Simosaurus* specimens were studied (Table 1). Usually, only samples taken exactly at midshaft were considered for the analysis of growth because they reveal the most complete growth record. However, the growth record of humerus SMNS 52095 that was sampled distal to midshaft is well preserved and seems to be fairly complete with only two or three annual growth cycles missing. Modelling this humerus revealed reasonable results. Thus, this sample was included into the analysis, but modelling results must be evaluated carefully. Femur SMNS 91983 was also sampled distally to the midshaft. Its annual growth record is, however, not very distinct, which means that growth cycles cannot be followed all around the cross section. Thus, annual cycles cannot unequivocally be distinguished from subcycles and this specimen was excluded from growth curve modelling.

For SMNS 18038, SMNS 18689, SMNS 18698, and SMNS 52095 four standard sigmoidal growth models were tested, which basically differ in the position of the inflection point: von Bertalanffy (c. 30% of asymptotic mass), Gompertz (c. 38%), logistic (50%), and Chapman-Richards growth model (not predefined, variable). The number of growth marks preserved in all specimens is small, but the standard growth models have a comparatively large number of parameters. Therefore, different versions for each of the four sigmoidal growth models were tested. These model versions differ in the number of model parameters estimated, e.g., in the model equation the parameter body mass at the first growth mark was set to zero or the parameter asymptotic body mass was set to the body mass at death of the specimen. The fully-parameterized von Bertalanffy growth model and the Gompertz model have three model parameters (body mass at the first growth mark M_0, asymptotic body mass A, and growth rate g), the logistic growth model has four parameters (body mass at the first growth mark M_0, asymptotic body mass A, growth rate g, growth mark at which the inflection point is located i), and the Chapman–Richards model has five parameters (body mass at the first growth mark M_0, asymptotic body mass A, growth rate g, parameters i and m set the position of the inflection point at the time and body mass axis). For each model version two model fitting techniques were used to estimate the number of missing growth cycles, to cope with the problem that in the inner part of the bone the growth record could be incomplete. For both techniques, a hatchling mass of 400 g was used based on histological data revealed from specimen SMNS 18698 (see Section 3). Under fitting technique 1 the number of missing cycles of a specimen was read off from the fitted growth curve at the age for which it predicts a mass of 400 g. Under fitting technique 2 the mass at cycle zero was set to a fixed hatchling weight of 400 g, and stepwise considered different numbers of missing cycles during model fitting (0, 1, ...) until the residual standard error and the AIC value stabilized (change < 1). In this paper, contrary to Griebeler et al. (2013), a linear growth model was also considered for each specimen in order to test whether its growth record only covers the quasi-linear phase of growth. Finally, for each specimen the statistically best supported model out of the set of candidate models was identified. First, their biological plausibility were checked (hatchling mass ≥ 0 and 400 g, asymptotic mass ≥ 0 and larger than hatchling mass, and growth rate ≥ 0), and next their residual standard errors for absolute goodness of fit, as well as their AIC scores, ΔAIC values, and Akaike weights for relative goodness of fit were evaluated. Fitting of growth curves and calculation of AIC

values was conducted in the free statistic software R (version 3.0.2) using the "nls"-function provided in the package "nls".

3. Results

3.1. Morphological description

The humerus of *Simosaurus* is a slender, curved bone with a rather simple morphology when compared to other Eosauropterygia (Fig. 1A, B) (Bickelmann and Sander, 2008; Klein, 2010; Rieppel, 1994). The proximal head is smooth and round, but with a straight preaxial margin due to the prominent development of the ventrally running deltopectoral crest. The proximal head forms ventropreaxially a flat surface that extends down to the midshaft. The proximal end is more massive and longer than the distal end. The distal end is wider than the proximal one but not as much expanded as in other Sauropterygia. The midshaft margins are straight and the area is slightly constricted. The proximal end is angled/twisted when compared to the midshaft/distal end resulting in a curvature of the entire bone. Humerus SMNS 52095 is complete, except for reconstructed parts of the distal end. It has a shallow groove that can be interpreted as an entepicondylar foramen (contrary to Rieppel, 1994) (Fig. 1A). The entire bone is heavily striated. Sampling location of this bone is not directly at the midshaft but slightly distally due to the presence of

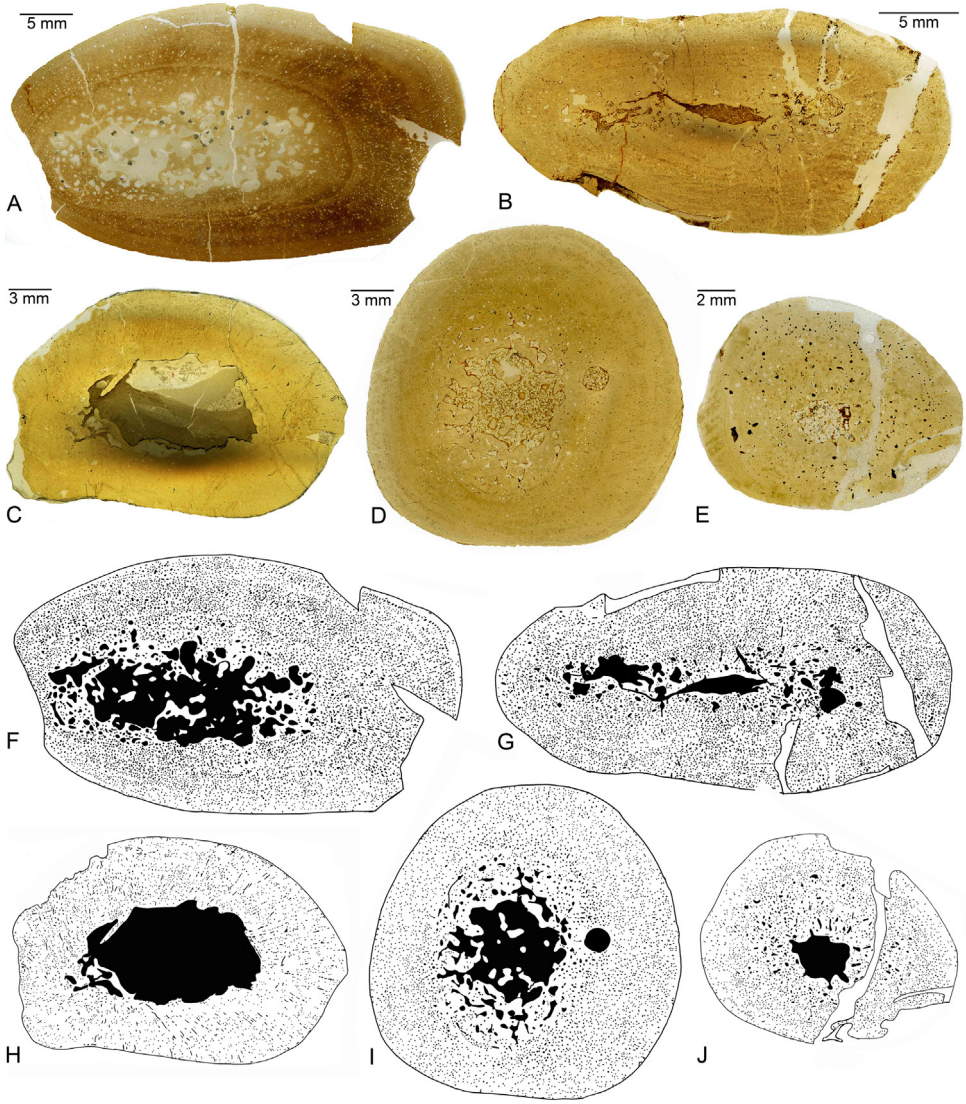

Fig. 2. (Color online.) Scanned cross sections (A–E) and modified black and white pictures (F–J) used for the microanatomical analysis of humeri and femora of *Simosaurus gaillardoti* from the Upper Muschelkalk of southern Germany. A, F. Humerus SMNS 52095. B, G. Humerus SMNS 18698; C, H. Femur SMNS 18689. D, I. Femur SMNS 91983. E, J. Femur SMNS 18038.
Fig. 2. (Couleur en ligne.) Coupes (A–E) scannées et modifiées en images en noir et blanc (F–J) utilisées pour l'analyse microanatomique d'humérus et de fémurs de *Simosaurus gaillardoti* du Muschelkalk supérieur d'Allemagne méridionale. A, F. Humérus SMNS 52095. B, G. Humérus SMNS 18698. C, H. Fémur SMNS 18689. D, I. Fémur SMNS 91983. E, J. Fémur SMNS 18038.

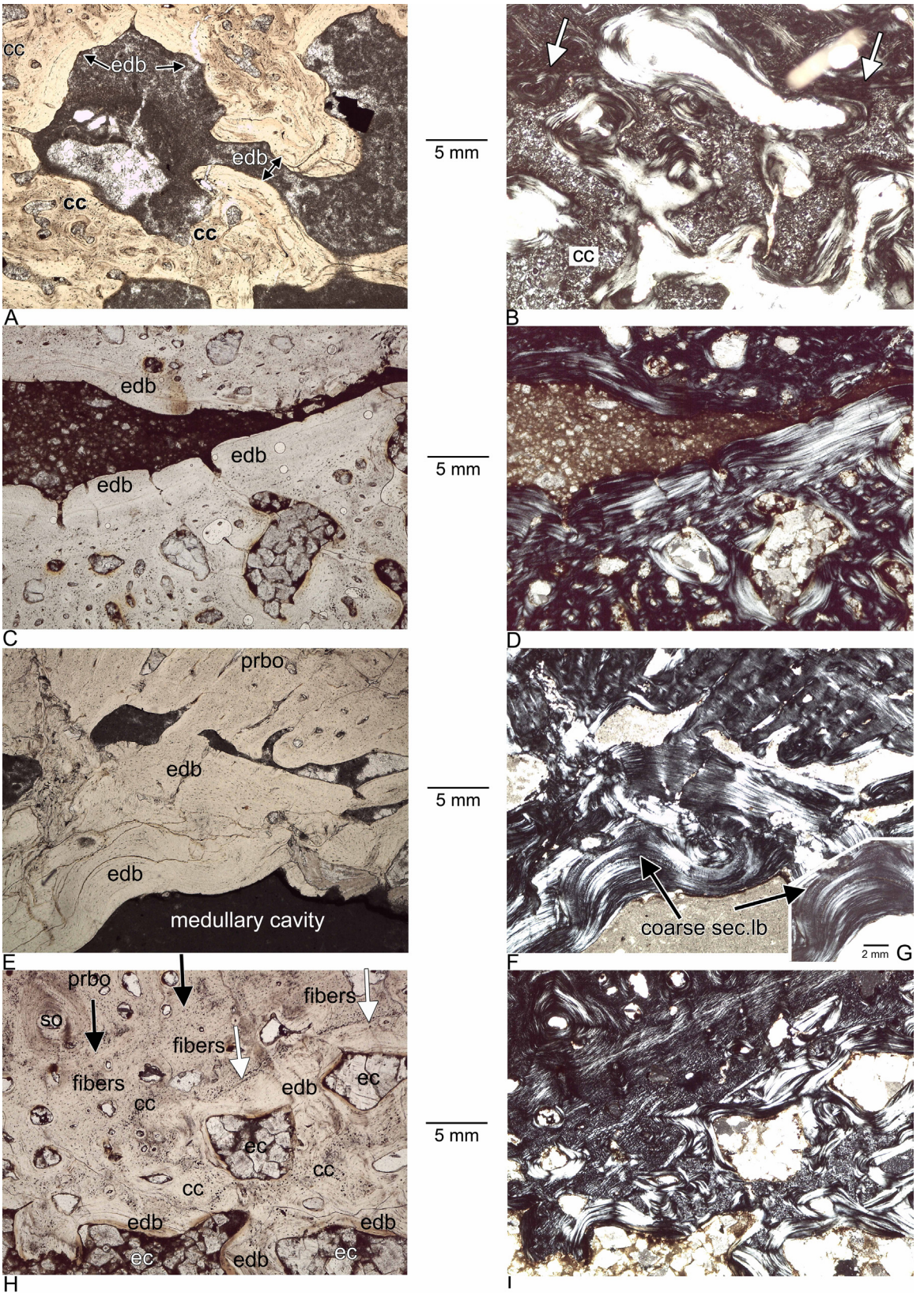
cc
edb
edb
cc
cc
A
5 mm
cc
B
edb
edb
edb
C
5 mm
D
prbo
edb
edb
medullary cavity
E
5 mm
coarse sec.lb
2 mm
F
G
prbo
so
fibers
fibers
fibers
edb
ec
cc
ec
cc
cc
edb
edb
ec
edb
ec
H
5 mm
I

plaster in the midshaft region. Humerus SMNS 18698 is also a complete bone with a few reconstructed areas. This humerus is heavily dorsoventrally flattened. The proximal end is much more angled (nearly 35°). It is disproportionate when compared to the midshaft and distal end of SMNS 52095. Distally, the humerus shows traces of oyster growth, indicating that the bone was for a while exposed before final burial/fossilization. Humeral cross sections are oval (Fig. 2).

The femur of *Simosaurus* is generally slender and only slightly curved (Fig. 1C, D, E). The midshaft region is clearly constricted. The prominent development of the trochanter results in a triangular cross section of the proximal head of the femur. The postaxial and dorsal margins of the proximal head are straight in dorsal view. The distal end is weakly broadened with the articular condyles being separated from each other by a shallow intercondylar fossa. This fossa separates the tibial and fibular articulations, which is not the case in other Eosauropterygia. SMNS 18689 is a complete femur that is ventrodorsally compressed. SMNS 91983 is the distal end of a femur with straight midshaft margins and two separated condyli. SMNS 18038 is a complete femur that resembles the morphology of SMNS 18689. Femur cross sections are round, except for SMNS 18038, where the cross section is oval (Fig. 2).

3.2. Microanatomical description

Due to different sampling locations along the midshaft the medulla of the sampled *Simosaurus* bones is variable. The distal sample of the largest humerus SMNS 52095 shows a medullary region surrounded by a spongeous perimedullary region (Fig. 2A, F). The midshaft sample of humerus SMNS 18698 has a prepostaxially elongated free medullary cavity surrounded by a narrow perimedullary region (Fig. 2B, G). The midshaft sample of femur SMNS 18689 and the midshaft sample of femur SMNS 18038 both share a central free cavity (Fig. 2C, E, H, J) and nearly no perimedullary region exists. Please note that the medullary cavity in SMNS 18038 is filled by crystallites (Fig. 2E). The distal sample of femur SMNS 91983 shows a large medullary region (Fig. 2D, I).

The medullary regions and cavities are surrounded by a moderately vascularized compacta. In general, vascularization is highest in the inner cortex and decreases towards the outer cortex. Vascular canals appear as primary osteons, immature primary osteons (Klein, 2010; Klein et al., 2015a), and simple vascular canals. Immature primary osteons are vascular canals, which are not completely lined by lamellar bone. Osteons are enlarged by erosion (secondary widening, see Klein et al., 2015a). Bone compactness of the cortex (without the medulla) revealed that vascular density is lower in femora than in humeri (Table 1). Bone compactness calculated with Bone Profiler (medulla included) revealed similar values for humeri and femora (Table 1) that result from the large medullary cavity/region in femora. Bone compactness ranges between 74.6% and 81.4% in humeri and between 73% and 88.5% in femora (Table 1). When the medulla is excluded from the calculation, bone compactness is around 90% in humeri and between 94.9% and 96.5% in femora (Table 1).

Femoral bone tissue is dominated by longitudinally organized canals, but radial canals can also occur. Femur SMNS 18689, for example, has a high amount of radial vascular canals that are mainly radially arranged along the cortex (Fig. 2C, H). In the humeri the organization and form of vascular canals are more variable than in the femora, but longitudinal canals dominate the tissue, as well. Most of the cortex of humerus SMNS 52095 is moderately vascularized by longitudinal canals, but locally the cortex is highly vascularized by a mixture of longitudinally, radially, and reticular arranged canals (Fig. 2A, F).

3.3. Histological description

The extensive medullary region of humerus SMNS 52095 consists of large cavities surrounded by endosteal (secondary) trabeculae and endosteal bone, the latter are not arranged in a trabecular structure. The endosteal deposits comprise large amounts of calcified cartilage (Fig. 3A, B). The area is surrounded by the typical sharp line that is a thin layer of lamellar (endosteal) bone, which is the boundary between the endochondral and periosteal domain (Klein, 2010; Klein et al., 2015a) (Fig. 3B, white arrow). Endochondral erosion has altered this boundary. Endosteal deposits reach into the periosteal domain. Secondary endosteal trabeculae comprise remains of primary bone obscuring the boundary between the endochondral and periosteal domain as well. The free medullary cavity of humerus SMNS 18698 is lined by a thick layer of endosteal bone (Fig. 3C, D) and endochondral remodeling has altered the inner cortex. The free cavities of femur SMNS 18689 and femur SMNS 18038 are both lined by a distinct layer of endosteal bone that locally reaches into the periosteal

Fig. 3. (Color online.) Histological details of the medulla of humeri and femora of *Simosaurus gaillardoti*. A, B. Medullary region of humerus SMNS 52095 in normal (A) and polarized light (B). C, D. Margin of the small medullary cavity of humerus SMNS 18698 in normal (C) and in polarized light (D). E, F. Margin of the large medullary cavity of femur SMNS 18689 in normal (E) and in polarized light (F). G. Enlargement of F showing coarse secondary lamellar bone. H, I. Margin of the large medullary cavity of femur SMNS 91983 in normal (H) and in polarized light (I). The white arrows mark the border between the endosteal and periosteal domain (sharp line). The black arrows mark an annulus, which separates the innermost cortex, here consisting of fibers, from the primary periosteal bone; abbreviations: cc: calcified cartilage; ec: erosion cavities; edb: endosteal bone; lb: lamellar bone; prbo: primary bone; so: secondary osteon.

Fig. 3. (Couleur en ligne.) Détails histologiques de la moelle de *Simosaurus gaillardoti*. A, B. Zone médullaire de l'humérus SMNS 52095 en lumière normale (A) et polarisée (B). C, D. Bordure de la petite cavité médullaire de l'humérus SMNS 18698 en lumière normale (C) et polarisée (D). E, F. Bordure de la grande cavité médullaire du fémur SMNS 18689 en lumière normale (E) et polarisée (F). G. Agrandissement de F montrant l'os lamellaire secondaire grossier. H, I. Bordure de la grande cavité médullaire du fémur SMNS 91983 en lumière normale (H) et polarisée (I). Les flèches blanches montrent la limite entre les domaines périostéal et endostéal (ligne fine). Les flèches noires indiquent un annulus qui sépare le cortex le plus interne, ici constitué de fibres, de l'os périostéal primaire ; abréviations: cc : cartilage calcifié ; ec : cavités d'érosion ; edb : os endostéal ; lb : os lamellaire ; prbo : os primaire ; so : ostéone secondaire.

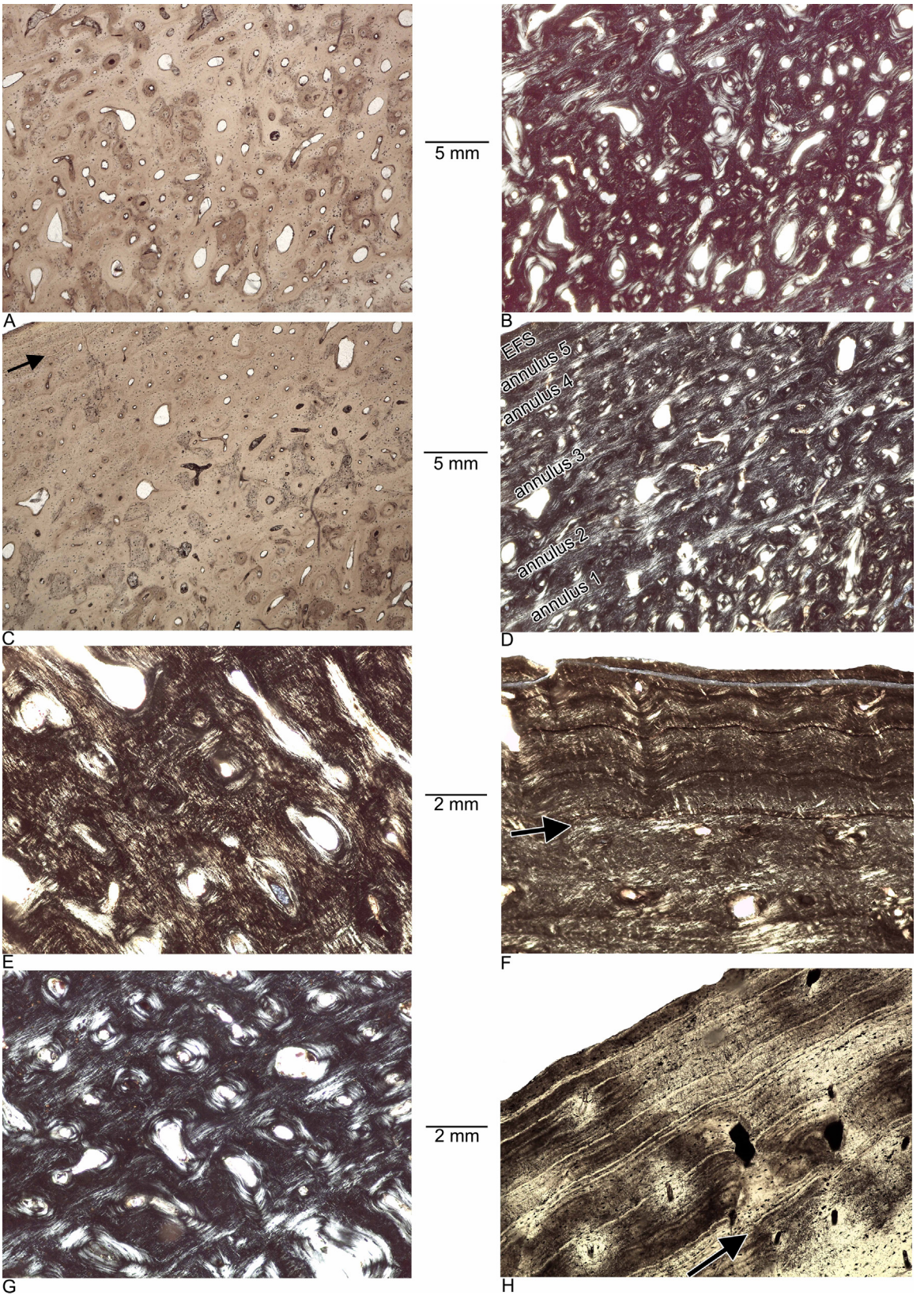
5 mm
5 mm
2 mm
2 mm
EFS
annulus 5
annulus 4
annulus 3
annulus 2
annulus 1
A
B
C
D
E
F
G
H

domain (Fig. 3E, F). The free medullary cavity of femur SMNS 18038 is additionally surrounded by a sharp line of endosteal bone comprising calcified cartilage as well as endosteal deposits. The large medullary region of femur SMNS 91983 is surrounded by a sharp line and consists of endosteal (secondary) trabeculae and of endosteal bone comprising large amounts of calcified cartilage (Fig. 3H, I).

In all samples, the cortex consists of a coarse parallel-fibred bone matrix with numerous osteocytes (Fig. 4A–D). Primary osteons are thickly lined by lamellar bone (Fig. 4A–E). Humerus SMNS 52095 shows an abrupt change in its outer cortex from coarse parallel-fibred bone to lamellar bone, resulting in an external fundamental system (EFS) (Fig. 4F). In femur SMNS 91983 an increase in tissue organization towards the outer cortex is visible, but no change to an EFS is observed. In femur SMNS 18689 and humerus SMNS 18698 (Fig. 4G) coarse parallel-fibred bone is interspersed with lamellar bone throughout the entire cortex resulting in a much higher tissue organization when compared to the other *Simosaurus* bones. The smallest femur SMNS 18038 also shows an EFS in its outer cortex (Fig. 4H). All femora have locally a funnel-shaped arrangement of the crystallites (only visible in polarized light) enclosing simple vascular canals (Fig. 5A, B) as was also described for nothosaur humeri by Klein (2010). Femur SMNS 91983 has a thick ring of fibers that surround the entire medullary region and immediately follow the sharp line (Fig. 5). The innermost part is made of a layer of angled fibers that is followed by a layer of longitudinally (rhombic appearance) arranged fibers and ends in a layer of smaller longitudinal fibers (Fig. 5D). The fibers are short and oblique, very dense and had replaced the primary periosteal bone tissue. Thus, no primary bone tissue is visible between these fibers.

Remodelling occurs in all samples and is reflected in the form of erosion of primary osteons (secondary widening). Mature secondary osteons i.e. largely infilled secondary osteons (Currey, 2002) are rare and intermixed with primary osteons and secondarily widened osteons, in which the lamellar bone still surrounds a large canal (Fig. 4).

3.4. Growth record

The cortex of *Simosaurus* is stratified by zones and annuli. Lines of arrested growth (LAGs) only occur within an EFS. Zones are identified as broad layers of vascularized and poorly organized coarse parallel-fibred bone tissue (Fig. 4D, G). Annuli are thin layers of highly organized and avascular bone tissue, consisting mainly of lamellar bone (Fig. 4D, G). The growth record in femora SMNS 18689 and SMNS 91983 is only locally preserved and not completely traceable along the cross section. Subcycles stratify the broad zones and resemble annuli (thin layers of avascular lamellar bone).

The growth record on which growth curve modelling was based, was measured on the ventral side of humeri SMNS 52095 and SMNS 18698 (Fig. 6A, B). After the fifth visible annulus, the tissue changes in SMNS 52095 to an EFS that contains five LAGs (Fig. 4C, F).

In femur SMNS 18689 the growth record is best preserved at the dorsopreaxial bone side (Fig. 6C). Annulus 3 and 4 each contain several resting lines (Fig. 6C, E, F). From annulus 6 onwards the annuli are regularly spaced. In femur SMNS 91983 the growth record is diffuse. Around five, more or less regularly spaced annuli are countable, but not traceable all around the cross section. They are additionally obscured by numerous subcycles throughout the entire cortex. The smallest sampled femur SMNS 18038 has the most distinct annual growth cycle record, which is preserved at its postaxial bone side (Fig. 6D). The growth cycle starts here with a broad zone that ends in an annulus. Between the second and the fourth growth cycle the zones and annuli are nearly equally broad (Fig. 6G, H). Growth cycle distance narrows down after the third visible growth cycle, possibly indicating the onset of sexual maturity. The zone of the fifth growth cycle consists only of a single row of vascular canals. The sixth and seventh growth cycles are embedded in an EFS and only recognizable under the microscope using polarized light (Fig. 6H).

3.5. Modelling of growth and comparison with histological data

For all specimens, the logistic, von Bertalanffy, and Gompertz growth models were successfully fitted to the growth record, but not all models were biologically realistic. The Gompertz models generally had negative growth rates, and the von Bertalanffy models obtained for SMNS 18689 and SMNS 18698 had negative growth rates and negative asymptotic masses (Table 2). For the Chapman-Richards growth model fitting always failed, presumably because of the large number of parameters of this model compared to the small number of annual growth cycles preserved.

The histological examination of humerus SMNS 52095 revealed ten visible annual growth cycles (Table 1). After

Fig. 4. (Color online.) Histological details of the cortexices of humeri and femora of *Simosaurus gaillardoti*. A–F. Humerus SMNS 52095. A, B. Coarse parallel-fibred bone in the inner cortex in normal (A) and in polarized light (B). C. Middle to outer cortex showing the transition to an EFS in normal light (black arrow). D. Showing alternating broad zones and thin annuli and the EFS in the outer cortex in polarized light. E. Detail of coarse parallel-fibred bone in polarized light. F. Detail of lamellar bone of the EFS in polarized light. The arrow marks the beginning of the bone tissue change. G. Femur SMNS 18698 in polarized light showing coarse parallel-fibred bone and alternating broad zones and thin annuli. H. EFS in the outer cortex of femur SMNS 18038 in normal light. The arrow marks the beginning of the bone tissue change. Please note that this picture is from the preaxial side, where the EFS contains more resting lines than at the postaxial bone side figured in Fig. 6D, G, H.

Fig. 4. (Couleur en ligne.) Détails histologiques des cortex d'humérus et de fémurs de *Simosaurus gaillardoti*. A–F. Humérus 52095. A, B. Os grossier à fibres parallèles dans le cortex interne en lumière normale (A) et polarisée (B). C. Cortex médian à externe montrant la transition vers un EFS en lumière normale (flèche noire). D. Montrant une alternance de zones larges et d'annuli minces et l'EFS dans le cortex externe en lumière polarisée. E. Détail de l'os grossier à fibres parallèles en lumière polarisée. F. Détail de l'os lamellaire de l'EFS en lumière polarisée. La flèche indique le commencement de la transformation du tissu osseux. G. Fémur SMNS 18698 en lumière polarisée montrant l'os grossier à fibres parallèles et l'alternance de larges zones et de minces annuli. H. EFS dans le cortex externe du fémur SMNS 18038 en lumière normale. La flèche indique le commencement de la transformation du tissu osseux. À noter que l'image est prise du côté préaxial, où l'EFS contient un plus grand nombre de lignes de repos que le côté post-axial de l'os, représenté sur la Fig. 6D, G, H.

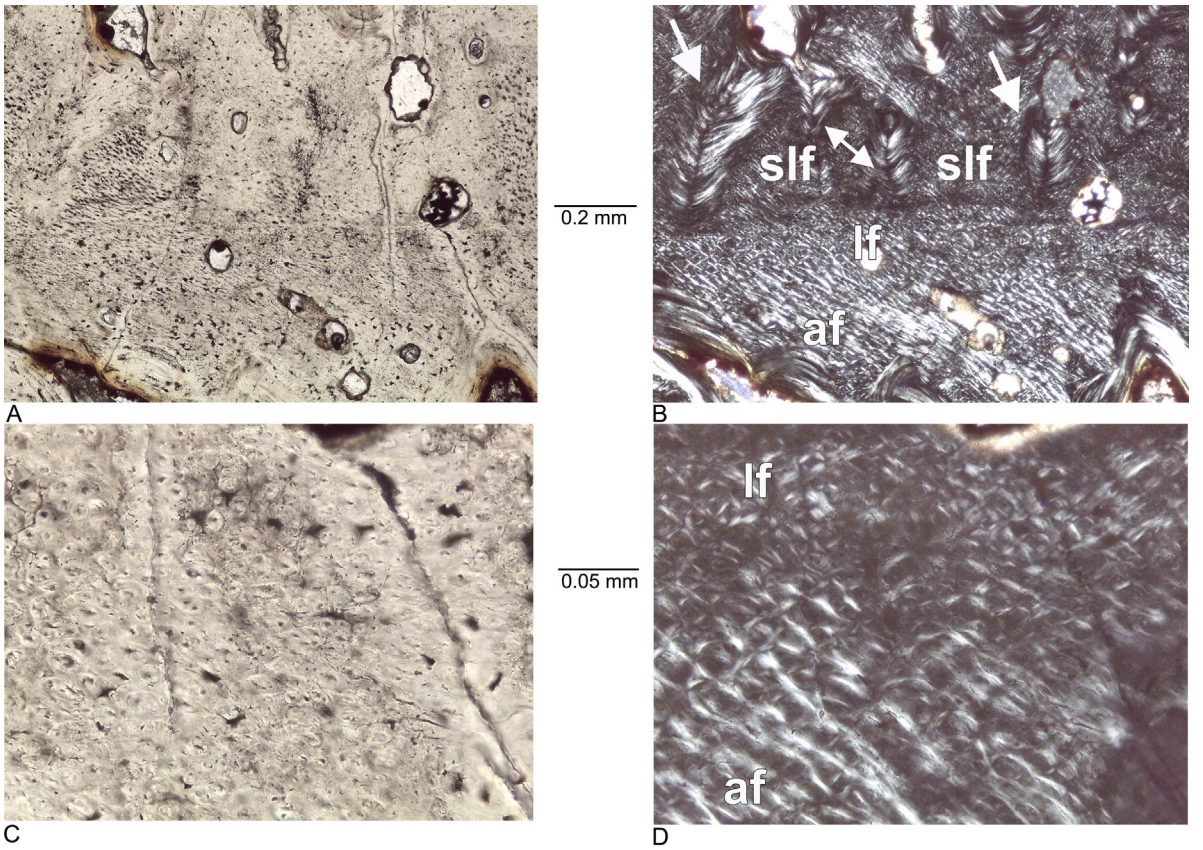

Fig. 5. (Color online.) Histological details of the inner tissue of femur SMNS 91983 of *Simosaurus gaillardoti*. A. Fibers between the medullary region (bottom of the picture) and the primary bone tissue in normal light. B. Same picture in polarized light, arrows mark funnel-shaped simple vascular canals. C, D. Enlargement of the fibers in normal (C) and in polarized light (D). Abbreviations: af, angled fibers; lf, longitudinal fibers; slf, small longitudinal fibers.
Fig. 5. (Couleur en ligne.) Détails histologiques du tissu interne du fémur SMNS 91983 de *Simosaurus gaillardoti*. A. Fibres entre la zone médullaire (bas de l'image) et le tissu osseux primaire en lumière normale. B. Même image en lumière polarisée, les flèches montrent les canaux vasculaires simples en forme d'entonnoir. C, D. Agrandissement des fibres en lumière normale (C) et polarisée (D). Abréviations : af, fibres obliques ; lf, fibres longitudinales ; slf, petites fibres longitudinales.

the fifth visible annual growth cycle an EFS is observed. Two or three annual growth cycles are lost in the inner part of the bone, which suggests that the individual was between 12 and 13 years old when it died. As no considerable decrease in growth rate is preserved in the mid cortex of this humerus, the onset of maturity is not documented. Growth in SMNS 52095 was best explained by logistic growth models that basically differ in the number of growth marks assumed that are lost in the growth center (Tables 1, 2; Figs. 6A, 7A). The logistic growth model assuming that no (one, two, and three) growth marks are lost had a low residual standard error of 6.4 (5.5, 5.4, 5.4) and a low AIC value of 70.0 (73.3, 72.8, 72.6). The best von Bertalanffy growth model provided a distinctly poorer fit (res. s.e. = 9.9 and AIC = 79.4). Statistically, none of the four logistic models is preferred over any other ($\Delta AIC \approx 2$, Burnham and Anderson, 2002). Hatchling mass predicted by the logistic model that assumes that no growth cycle is missing was 8.68 ± 0.1 kg (s.e., standard error), which is unrealistic high compared to the hatchling mass of c. 400 g suggested by specimen SMNS 18698 (see below). It was zero and thus much closer to this hatchling mass under the other three logistic models. Estimated asymptotic mass did only slightly differ between fitted models, and ranged from 117.1 ± 4.1 kg (no cycle is missing) to 119.3 ± 3.8 kg (three cycles are missing). The ages at death predicted by the models ranged between 10 and 13 years, and the ages at which asymptotic mass is reached between 10 and 13 years, too, which is consistent with the presence of an EFS in the histological record. All models located the inflection point between the third and fourth growth mark, which would coincide with an onset of reproductive maturity between 3–4 years up to 6–7 years. The maximum growth rate for this bone was within its fourth year of life and was between 64 and 65 g per day (23.2 and 25.2 kg per year).

The small medulla in humerus 18698 suggests that the growth record is complete and no annual growth cycle is missing in its innermost cortex. Seven annual growth cycles are preserved suggesting that the individual died in its eighth year of life. As no EFS is documented in the bone, this individual was not in the asymptotic phase of growth when it died. The considerable decrease in growth

Table 2
Growth models obtained for humeri and femora studied. For each standard growth model successfully applied the best versions of models are shown.
Tableau 2
Modèles de croissance obtenus à partir des humérus et fémurs étudiés. Pour chaque modèle de croissance standard appliqué avec succès, les meilleures versions des modèles sont présentées.

Bone spec. no.	Model	#miss. gms (year)	M_0 (kg)	s.e.	A (kg)	s.e.	g (kg per year)	s.e.	i (year)	s.e.	Res. s.e.	df	AIC	df	ΔAIC_1	w_1 (ΔAIC) (%)	ΔAIC_2	w_2 (ΔAIC) (%)
Humerus SMNS 52095	LM		12.5$^{n.s.}$	6.4			13.910$^{n.s.}$	8.152			10.92	8	80.0	3	9.9	0.7	7.4	2.4
	vBGM	0	0 (fix)		184.8***	35.3	0.131*	0.039			9.86	8	79.4	3	9.3	0.9	6.8	3.2
	GGM	0	33.8**	7.5	126.3 (fix)		−0.166***	0.031			18.98	8	91.0	3	–	–	–	–
	LGM	0	8.7***	0.3	117.1***	4.1	0.957***	0.144	3.3***	0.192	6.44	7	70.1	4	0	98.4		
	LGM	3	0 (fix)		119.3***	3.8	0.804***	0.093	6.1***	0.169	5.36	8	72.6	4			0	94.4
Humerus SMNS 18698	LM		−6.5 $^{n.s.}$	4.6			13.705***	1.280			6.77	5	50.9	3	14.2	0.1		
	vBGM	0	0 (fix)		−46305.9***	4519.6	−0.229***	0.013			1.06	5	24.3	3	–	–	–	–
	GGM	0	7.9***	1.4	84.4 (fix)		−0.402***	0.034			4.51	5	44.6	3	–	–	–	–
	LGM	0	0.6***	0.1	125.7**	20.7	0.674**	0.082	5.0***	0.542	2.48	4	36.6	4	0	99.9		
Femur SMNS 18689	LM		0.3$^{n.s.}$	2.0			12.480 $^{n.s.}$	6.899			3.67	8	58.2	3	0	84.1	0	54.6
	vBGM	3	0 (fix)		−85229.8*	30700.4	−0.117***	0.024			5.26	9	67.9	3	–	–	–	–
	GGM	3	10.3**	2.3	113.4 (fix)		−0.213***	0.021			9.13	9	83.7	3	–	–	–	–
	LGM	0	7.7***	0.5	113.5***	6.9	0.589***	0.063	5.2***	0.334	4.20	7	61.5	4	3.3	15.9		45.4
	LGM	3	0 (fix)		129.2***	6.7	0.490***	0.037	8.2***	0.283	2.82	8	58.5	4			0.3	
Femur SMNS 18038	LM		15.3**	2.7			10.458**	1.825			3.93	5	42.7	3	13.6	0.1		
	vBGM	0	10.5**	1.5	109.1***	15.4	0.172**	0.031			1.44	4	29.1	4	0	99.7		
	GGM	0	21.0**	3.4	73.4 (fix)		−0.218**	0.039			8.45	5	53.4	3	–	–		
	LGM	0	13.1***	0.5	73.0***	3.9	0.943	0.163	2.325	0.256	3.63	4	42.0	4	12.9	0.2		

LM: linear model (test for quasi-linear phase of growth); vBGM: von Bertalanffy growth model; GGM: Gompertz growth model; LGM: logistic growth model); please note that the Chapman-Richards growth model could not successfully fitted to any of the bones; #miss. gms: number of missing growth marks in the inner cortex predicted by the model; M_0: hatchling mass; A: asymptotic mass; g: growth rate; i: location of the inflection point on the x-axis; s.e.: standard error of an estimated model parameter value; residual s.e.: residual standard error of the model (absolute measure of its goodness of fit); AIC: AIC value of the model (relative measure of its goodness of fit, Burnham and Anderson, 2002); ΔAIC: $AIC_{model} - minAIC$ (Burnham and Anderson, 2002); $w(\Delta AIC)$: Akaike weights (normalized relative model likelihoods, Burnham and Anderson, 2002); df: degrees of freedom. For humerus SMNS 52095 and femur SMNS 18689 four LGMs differing in the number of missing growth marks (0, 1, 2, or 3) were equally well supported in terms of AIC values. Equations of growth functions are LM: $M(t) = M_0 + gt$, vBGM: $M(t) = \left(\sqrt[3]{A} - (\sqrt[3]{A} - \sqrt[3]{M_0})\exp(-gt)\right)^3$, GGM: $M(t) = M_0 + A\exp(-\exp(-gt))$, and LGM: $M(t) = M_0 + \frac{A}{1+\exp(-g(t-i))}$. Please note that, in the sigmoidal equations, M_0, A, and g have to be positive numbers. Significance levels: $^{*}p \leq 0.05$, $^{**}p \leq 0.01$, $p \leq 0.001$, n.s. > 0.05.

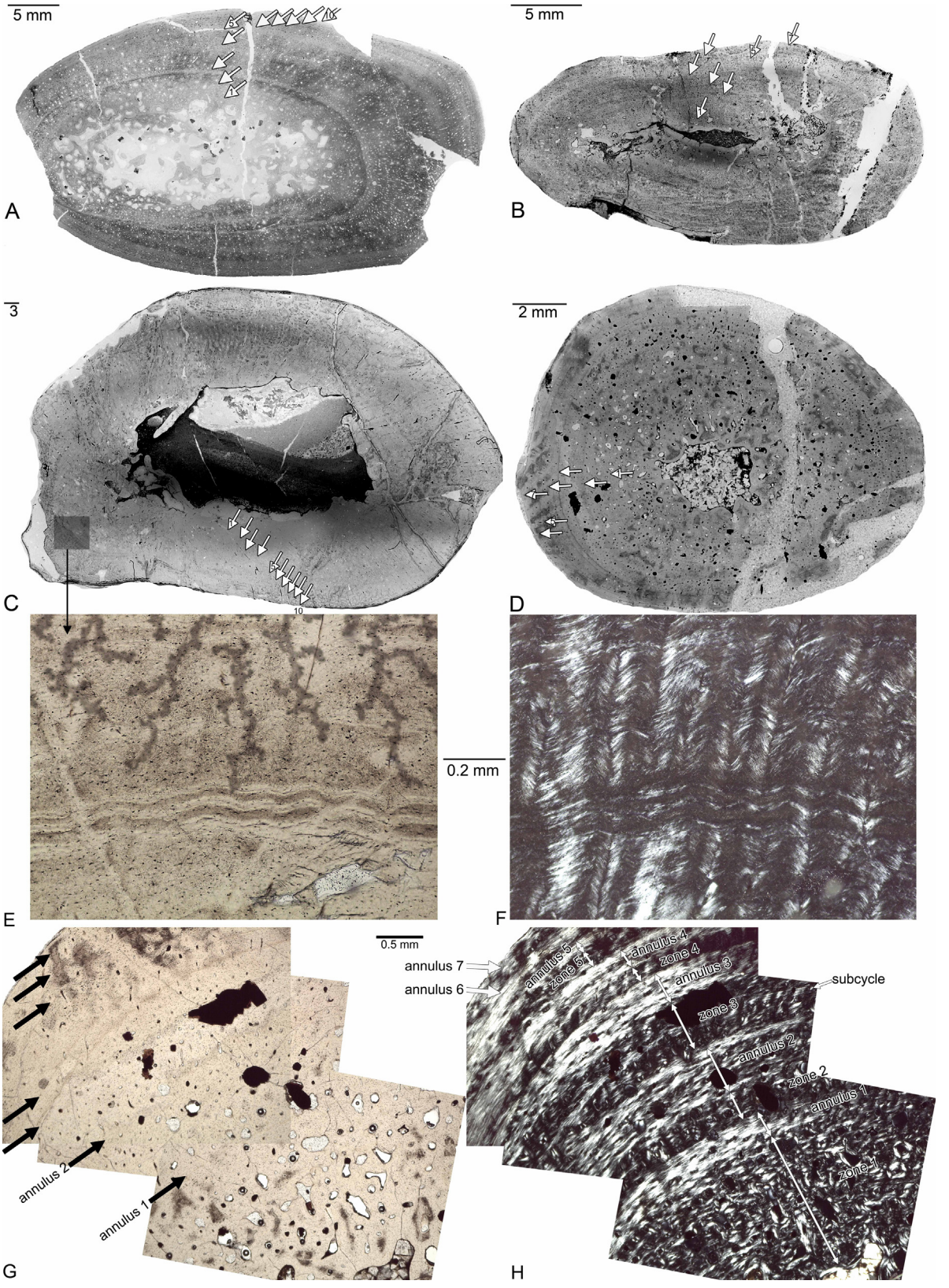
5 mm
A
5 mm
B
3
C
2 mm
D
10
0.2 mm
E
F
0.5 mm
annulus 7
annulus 6
annulus 2
annulus 1
G
annulus 5
zone 5
annulus 4
zone 4
annulus 3
subcycle
zone 3
annulus 2
zone 2
annulus 1
zone 1
H

rate after the second annual growth cycle could indicate sexual maturity. Growth in the humerus SMNS 18698 was clearly in terms of absolute and relative goodness of fit best described by a logistic model assuming that no growth mark is missing (Table 1, 2; Fig. 7A). This model estimated a hatchling mass of 570 ± 100 g, and an asymptotic mass of 125.7 ± 20.7 kg. The age at death of the individual is seven years and thus considerably lower than the age at which asymptotic mass is reached, which is 16 years. The inflection point of this logistic growth model is located between the fifth and sixth year of life, and thus does not coincide with the considerable decrease in growth observed after the second annual growth cycle. Maximum growth rate was within its sixth year of life and was 56 g per day (20.4 kg per year).

The histological examination of femur SMNS 18689 revealed ten annual growth cycles. Extrapolation suggested that three annual growth cycles are missing in the inner part of the bone. Thus, the individual was 13 years old when it died. After visible annulus 6 the growth marks are regularly spaced, but no EFS is visible. Four logistic models differing in the number of missing cycles assumed (0 up to 3 cycles) are well preferred over the linear model (quasi-linear phase of growth) due to their lower residual standard errors (Table 2). Contrary, the AIC based model selection indicated a very small support of the linear model over the logistic models in general and especially over the logistic model assuming that three growth cycles are missing (ΔAIC = 0.3; Table 2). The latter logistic model assumed a hatchling mass of zero, which is actually wrong from a biological point of view, but we think still tolerable when modelling growth for two reasons. First, the hatchling mass in *Simosaurus* is c. 400 g (as suggested by SMNS 18698 in which the first annual growth cycle is preserved) and thus small. Second, the estimated asymptotic masses of all specimens are two orders of magnitude larger than the hatchling mass. The estimated asymptotic mass of the SMNS 18689 individual derived from this logistic growth model is 129.2 ± 6.7 kg and its estimated age at death is 12 years. Its age at which asymptotic mass is reached is 20 years and thus consistent with bone histology as asymptotic age is considerably higher than the age at death. The inflection point (= onset of sexual maturity) of this logistic growth model is located between the sixth and seventh year. This suggests that the individual reached sexual maturity within its ninth year of life. The maximum growth rate derived from the logistic model is within its ninth year of life and is 44 g per day (15.9 kg per year). In total, for SMNS 18689 a best growth model was not unequivocally identified. Sigmoidal models assume a phase of acceleration of growth followed by a phase of deceleration of growth during the life of an individual. None of these phases is clearly documented in the growth record of SMNS 18698 as growth marks are missing in the inner part of the bone and the individual died before it reached the phase of growth deceleration.

The histological examination of femur SMNS 18038 revealed seven annual growth cycles. Extrapolation suggested that one cycle is missing in the inner part of the bone, and thus estimates that the individual died during its ninth year of life. After the fifth growth mark, an EFS is documented in the bone. Contrary to the other three bones, for which the logistic growth model was more or less preferred over the von Bertalanffy model, growth in SMNS 18038 was clearly best explained by a von Bertalanffy growth model in terms of absolute and relative goodness of fit (Table 2; Fig. 7A). This is unexpected as the number of growth marks documented in the bone is small (seven), and the AIC based model selection approach favors models with fewer parameters (two for the linear model) over models with more parameters (three for the von Bertalanffy model). The von Bertalanffy model predicts that no annual growth cycle is missing in the inner part of the bone, but estimates an unrealistic high hatchling mass of 10.5 ± 1.5 kg compared to c. 400 g suggested by SMNS 18698. The model predicts an age at death of seven years. The estimated asymptotic mass of the individual is 109.1 ± 15.4 kg, which is reached by the individual after 20 years of life. The inflection point of the growth model is located between the first and second year, which contradicts the histological examination, and is inconsistent with the ages at sexual maturity found for the other specimens (Table 1). However, this reflects the general earlier sexual maturity under a von Bertalanffy (age at which 30% of the asymptotic mass is reached) than under a logistic growth model (age at which 50% of the asymptotic mass is reached). The maximum growth rate for this bone was within its second year of life and was 36 g per day (13.1 kg per year). That SMNS 18038 follows the von Bertalanffy growth model could be related to its earlier ontogenetic stage and the absence of a sufficient number of growth marks documenting the asymptotic phase of growth. However, different individuals from a single species can follow different growth models (Frazer and Ehrhart, 1985; Halliday and Verrell, 1988; Magnusson and Sanaiotti, 1995; Ritz et al., 2010). This reflects developmental plasticity or variability in growth due to differences in exogenous (climate, food or water availability) and endogenous factors (stress, diseases) experienced by individuals. Although all *Simosaurus* bones sampled originate from bone beds and were thus not found together with diagnostic skull material, an incorrect taxonomical assignment of SMNS 18038 can be excluded. Long bone morphology of *Simosaurus* differs distinctly from that of other Euauropterygia found at the same localities (Rieppel, 1994, 2000).

Fig. 6. (Color online.) Annual growth cycles in humeri and femora of *Simosaurus gaillardoti* each marked by arrows. A. Humerus SMNS 52095. B. Humerus SMNS 18698. C. Femur SMNS 18689. D. Femur SMNS 18038. E, F. Enlargement of the third annulus of femur SMNS 18689 that at this bone side contains three subcycles in normal (E) and in polarized light (F). G, H. Detail of growth record in femur SMNS 18038.

Fig. 6. (Couleur en ligne.) Cycles de croissance annuels dans le cas des humérus et fémurs de *Simosaurus gaillardoti*. A. Humérus SMNS 52095. B. Humérus SMNS 18698. C. Fémur SMNS 18689. D, Fémur SMNS 18083. E, F. Agrandissement du troisième annulus du fémur SMNS 18689 qui, de ce côté de l'os, contient trois sous-cycles en lumière normale (E) et polarisée (F). G, H. Détail de l'enregistrement de la croissance dans le fémur 18038.

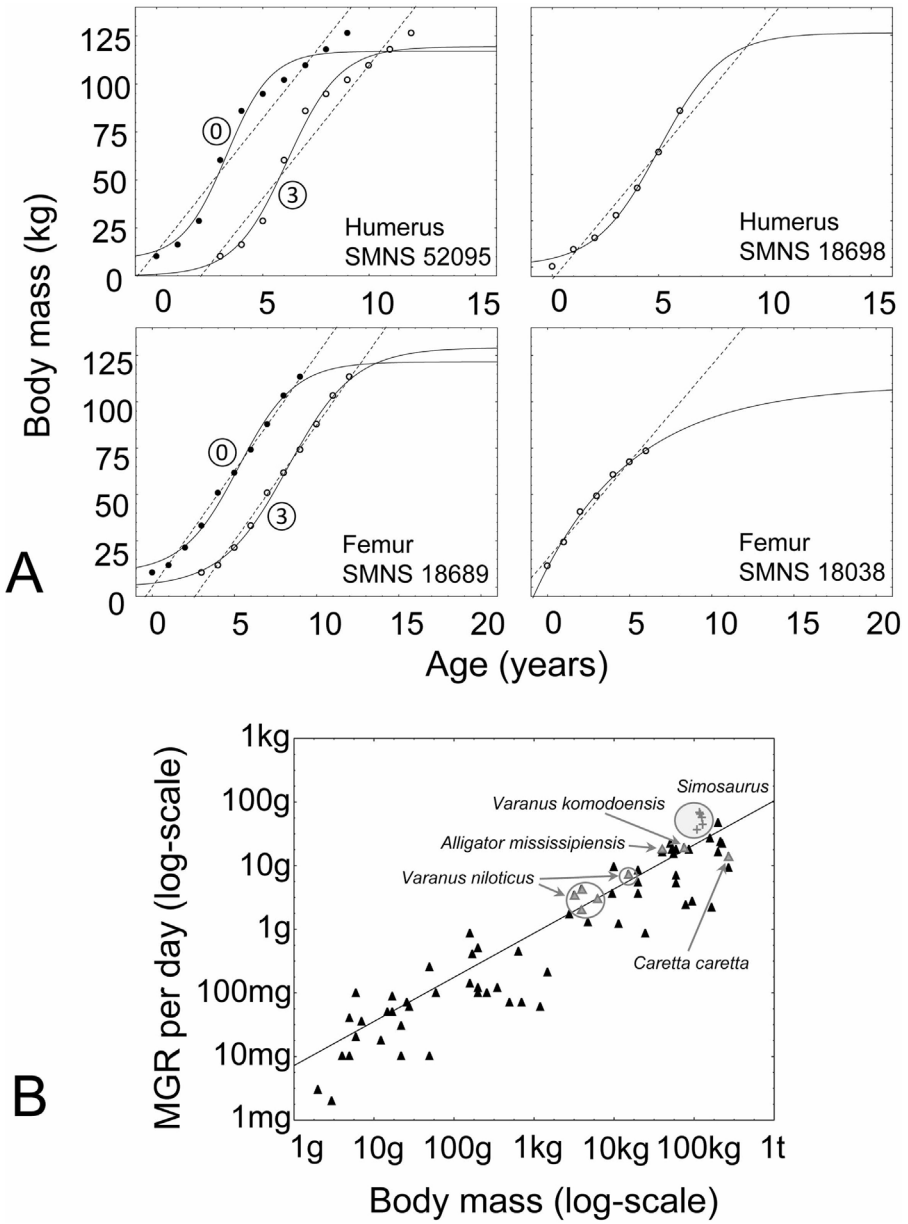

Fig. 7. (Color online.) A. Growth curves established for *Simosaurus gaillardoti*. For each individual the linear model (dotted lines) and the best sigmoidal growth model(s) (solid lines) are shown. For humerus SMNS 52095 and humerus SMNS 18698 four logistic growth models were equally supported in terms of AIC values. These models differed in the estimated numbers of missing cycles (0, 1, 2, or 3). Here only two of these four logistic growth models are shown. They assume that either no growth cycle is missing (minimum) or that three cycles (maximum) are missing. For femur SMNS 18689 and femur SMNS 18038 one sigmoidal growth model was identified and is shown. Parameter values of all sigmoidal growth models derived for specimens are summarized in Table 2. B. Comparison of maximum growth rates in *Simosaurus gaillardoti* to those of extant reptiles. Maximum growth rates (MGR) of extant species (triangles) and regression line on extant species are taken from Werner and Griebeler (2014). For *Simosaurus* growth rates were derived from the sigmoidal growth models (Fig. 7A, Table 2). *Simosaurus* had higher maximum growth rates than similar-sized average extant reptiles (regression line). Maximum growth rates of *Simosaurus* are higher than rates of extant large semi-aquatic species (i.e., *Varanus komodoensis* body mass = 87 kg and maximum growth rate = 18 g per day, *Alligator mississippiensis* 76 kg and 19 g per day, *Caretta caretta* 225 kg and 22 g per day; grey triangles). They are also higher than those observed in the much smaller semiaquatic *Varanus niloticus* (body mass = 3.2 kg and maximum growth rate = 3.4 g per day, 3.9 kg and 4.3 g per day, 3.9 kg and 2 g per day, 6.3 kg and 3 g per day, 15.2 kg and 7.3 g per day), even if the growth rates of *Varanus niloticus* are extrapolated to the mass of *Simosaurus*. Nevertheless, maximum growth rates of *Simosaurus* are still consistent with the variability seen in the maximum growth rates of extant reptiles.

Fig. 7. (Couleur en ligne.) Courbes de croissance établies pour *Simosaurus gaillardoti*. Pour chaque individu, le modèle linéaire (lignes tiretées) et le(s) meilleur(s) modèle(s) de croissance sigmoïdaux (lignes continues) sont indiqués. Pour les humérus SMNS 52095 et SMNS 18698, quatre modèles logistiques de croissance peuvent être tous également étayés en termes de valeurs AIC. Ces modèles diffèrent dans les nombres estimés de cycles manquants (0, 1, 2 ou 3). Ici ne sont montrés que deux de ces quatre modèles logistiques de croissance. Ils supposent que, soit aucun cycle de croissance n'est manquant (0 minimum), soit trois cycles (3 maximum) sont manquants. Pour les fémurs SMNS 18689 et SMNS 18038, un modèle sigmoïdal de croissance a été déterminé et est présenté. Les valeurs paramétrées de tous les modèles de croissance sigmoïdaux dérivés pour les

4. Discussion

4.1. Microanatomy

Simosaurus humeri and femora show exactly at midshaft a free medullary cavity. Distally or proximally to the midshaft the bones have a medullary region dominated by secondary trabeculae, which is also seen in placodonts (Klein et al., 2015a). The medullary cavities are lined by a thick layer of endosteal bone and are surrounded by a thick compacta, both resulting in bone mass increase, and more specifically osteosclerosis (Houssaye, 2009), when compared to terrestrial tetrapods. Osteosclerosis is also evident due to the presence of extensive calcified cartilage (incomplete endochondral ossification) in Simosaurus along the midshaft (Ricqlès and Buffrénil, 2001), (Figs. 3, 4, 5A, B). Although our sample size is limited, there is evidence that the medullary cavity in *Simosaurus* is larger in femora than in humeri, a tendency that is also documented in placodonts (Klein et al., 2015a, 2015b). Medullary cavities in humeri and femora are equally large in the pachypleurosaur *Anarosaurus heterodontus* (Klein, 2010, 2012), but always larger in humeri of the Upper Muschelkalk nothosaurs than in their femora (Klein, 2010; Krahl et al., 2013), which indicates different swimming styles. Microanatomical differences between the humeri and femora in *Simosaurus* indicate different functional requirements for both elements. This can be expressed for example, in that the humerus is more intensively used during swimming (e.g., for propulsion) than the femur.

A Principal Component Analyses (PCA) plot, which is based on Bone Profiler values and which included three *Simosaurus* midshaft samples (humerus SMNS 18698, femur SMNS 18038, femur SMNS 18689) as well as other aquatic extinct and extant taxa revealed different microanatomical clusters (Klein et al., 2015a: figure 8). Herein the *Simosaurus* humerus SMNS 18698 plots close to the marine reptile *Horaffia*, Placodontia indet aff. *Cyamodus*, *Pistosaurus*, and the pachypleurosaur *Anarosaurus heterodontus*. This group again is clearly separated from the Upper Muschelkalk nothosaurs as well as from the other aquatic taxa included that are highly or poorly efficient swimmers. Due to the difference in the size of their medullary cavities, both femora of *Simosaurus* generally have a large distance in this plot. Additionally, their distance to the femora of nothosaurs from the Upper Muschelkalk is large. Thus, microanatomical analysis suggests that *Simosaurus* has had certain active swimming skills as presumed for the above mentioned taxa, but was less efficient when compared to contemporaneously living and similar sized nothosaurs from the Upper Muschelkalk. If it was "capable of sustained swimming" (Rieppel, 1994: 1) was neither confirmed nor contradicted by the analysis of Klein et al. (2015a).

4.2. Histology

The most distinct feature of *Simosaurus* long bone histology is the coarse parallel-fibred bone tissue that is well interspersed with numerous and thick osteocytes (Fig. 4). Coarse parallel-fibred bone was recently described for some placodonts (Klein et al., 2015a) and for the temnospondyl *Plagiosaurus* (Konietzko-Meier and Schmitt, 2013). Houssaye et al. (2013) described an unusual parallel-fibred bone for mosasaurs. In placodonts, this coarse parallel-fibred tissue is intermixed with woven bone in a fibro-lamellar bone tissue. *Plagiosaurus* shows in its deepest cortex woven bone and immature primary osteons forming incipient fibro-lamellar bone (Klein, 2010; Konietzko-Meier and Schmitt, 2013), whereas neither mosasaurs (Houssaye et al., 2013) nor *Simosaurus* show fibro-lamellar bone. Houssaye et al. (2013) related the unusual parallel-fibred bone of mosasaurs to an increase in growth rate, an interpretation that is also realistic for *Simosaurus*. The presence of modified parallel-fibred bone tissue in mosasaurs and *Simosaurus* thus could represent a kind of pre-stage in the formation of fibro-lamellar bone. Coarse parallel-fibred bone is so far restricted to aquatic tetrapods. Some terrestrial taxa show a modification of the fibro-lamellar complex by parallel-fibred bone. This was described for early pseudosuchian archosaurs (Ricqlès et al., 2003), the ornithopod dinosaur *Gasparinisaura* (Cerda and Chinsamy, 2012), and the titanosaur dinosaur *Ampelosaurus* (Klein et al., 2012a). In all these taxa the woven bone component of the fibro-lamellar complex was replaced or modified (intermixed) by parallel-fibred bone, resulting in a lower growth rate.

The bone tissue type of *Simosaurus* can be categorized as lamellar-zonal, although it is not typical lamellar-zonal when compared to modern amphibians and reptiles. This is mainly due to its moderately high vascular density and due to the presence of coarse parallel-fibred bone. Although similar to nothosaurs (Klein, 2010; NK pers. obs.) *Simosaurus* has a unique combination of bone tissues as well as vascular density and organization when compared to other Sauropterygia (e.g., Hugi, 2011; Hugi et al., 2011; Klein, 2010, 2012; Klein et al., 2015a, 2015b; Krahl et al., 2013; Ricqlès and Buffrénil, 2001; Sander, 1990; Wiffen et al., 1995).

échantillons sont résumées dans le Tableau 2. B. Taux de croissance maximums chez *Simosaurus gaillardoti*, comparés à ceux de reptiles vivants. Les taux de croissance maximums (MGR) d'espèces existantes (triangles) et la ligne de régression sur les espèces existantes sont empruntés à Werner et Griebeler (2014). Pour *Simosaurus*, les taux de croissance sont dérivés des modèles sigmoïdaux de croissance (Fig. 7A, Tableau 2). *Simosaurus* a des taux de croissance maximums supérieurs à ceux de reptiles vivants de taille moyenne similaire (ligne de régression). Les taux de croissance de *Simosaurus* sont supérieurs à ceux des espèces vivantes semi-aquatiques de grande taille (par exemple : *Varanus komodoensis* a une masse corporelle de 87 kg et un taux de croissance maximum de 18 g par jour, *Aligator mississippiensis* a une masse corporelle de 76 kg et un taux de croissance maximum de 19 g par jour, *Caretta caretta* a une masse corporelle de 225 kg et un taux de croissance maximum de 22 g par jour (triangles gris). Ils sont aussi plus élevés que ceux observés chez *Varanus niloticus*, semi-aquatique beaucoup plus petit (masse corporelle = 3,2 kg et taux de croissance maximum = 3,4 g par jour, 3,9 kg et 4,3 g par jour, 3,9 kg et 2 g par jour, 6,3 kg et 3 g par jour, 15,2 kg et 7,3 g par jour), même si les taux de croissance de *Varanus niloticus* sont extrapolés par rapport à la masse de *Simosaurus*. Néanmoins, les taux de croissance maximums de *Simosaurus* sont encore compatibles avec la variabilité observée dans les taux de croissance maximums des reptiles vivants.

The thick inner ring composed of three successive layers of fibers (angled, large longitudinal, small longitudinal) in femur SMNS 91983 is very peculiar. None of the other *Simosaurus* samples shows a comparable fiber deposition. These fibers do not represent Sharpey's fibers, which are long, run through different bone layers and represent muscle and tendon attachments of gross morphology. In temnospondyls, similar fibers as described above for SMNS 91983 are interpreted as attachment fibers of the periost (Konietzko-Meier and Klein, 2013; Witzmann, 2009) or as ossified tendons in the cervical ribs in sauropod dinosaurs (Klein et al., 2012b). However, these explanations are not satisfying here. A pathological reason such as a false posture or a deficiency in early ontogeny of this individual could be a more likely explanation. The femur itself, however, does not show any abnormalities such as a healed break that would be indicated by a callus.

4.3. Growth and growth rate

In general, annual growth cycles in *Simosaurus* consist of broad zones alternating with thin annuli. Two bones show an EFS in their outer cortex. However, a certain variability and developmental plasticity in the sequence and spacing of growth marks of individuals are obvious, which is similar to the variation observed in placodonts (Klein et al., 2005b). In femur SMNS 18689 two annuli contain several resting lines indicating several cessations of growth during these two slow annual growth phases. These additional cessations of growth during an annual growth cycle can be the result of exogenous (climate, food or water availability) or endogenous factors (stress, diseases). Non-annual growth marks are known from many modern amphibians and reptiles (e.g., Castanet, 1994; Castanet et al., 1993). Additional non-annual resting lines within a single annulus are described in extinct taxa. They were observed in placodonts (Klein et al., 2015b) and in the temnospondyl *Metoposaurus* (Konietzko-Meier and Klein, 2013).

Hugi and Sánchez-Villagra (2012) report that marine iguana *Amblyrhynchus cristatus* had thicker zones than annuli before sexual maturity was reached, whereas zones were equally broad after the onset of sexual maturity, documenting that growth mark expressions can also depend on endogenous factors such as reproduction. A similar change in the proportion between zones and annuli is documented in femur SMNS 18038. However, the possibility that this change in proportion reflects the onset of sexual maturity remains questionable here (see above; Table 1).

Two approaches are applied to compare growth rates of *Simosaurus* to that of other marine and extant reptiles. First, bone tissue type as well as vascular density and organization of *Simosaurus* were compared to those of other Sauropterygia and marine reptiles, which both being a proxy for growth rates. Low tissue organization and high vascular density as well as the presence of radial vascular canals and a radial vascular canal organization indicate high growth rates in *Simosaurus* (e.g., Margerie et al., 2004; Ricqlès, 1976). These histological characters suggest that the growth rate of *Simosaurus* was intermediary between those of other sauropterygians and marine reptiles. Compared to nothosaurs, the tissue organization was lower due to the presence of coarse parallel-fibered bone and vascular density was increased in *Simosaurus* (Table 1; Hugi, 2011; Klein, 2010; Krahl et al., 2013; NK pers. obs.). Compared to the pachypleurosaurs *Neusticosaurus* spp., (Hugi et al., 2011; Sander, 1990) that have parallel-fibred bone and show a mainly longitudinal vascular canal organization, *Simosaurus* had higher growth rates. The bone tissues of *Simosaurus* were more organized and vascular density was lower when compared to the pachypleurosaur *Anarosaurus*, because the latter grew with incipient fibrolamellar bone and show a high amount of radial vascular canals (Table 1; Klein, 2010, 2012). Bone tissues and vascular canal organization of *Simosaurus* were similar to mosasaurs (Houssaye et al., 2013), but much lower when compared to placodonts (Buffrénil and Mazin, 1992; Klein et al., 2015a) or ichthyosaurs (Buffrénil and Mazin, 1990; Houssaye et al., 2014) both taxa having highly vascularized fibro-lamellar bone.

Second, maximum growth rates were estimated from the inflection point of fitted growth curves (Fig. 7A). These growth rates are compared to those of extant reptile species (Fig. 7B, regression line and species-specific maximum growth rates, data from Werner and Griebeler, 2014). The marine reptile *Simosaurus* exhibits a higher maximum growth rate when compared to modern average reptiles (Fig. 7B; Werner and Griebeler, 2014), which is also seen in other extinct marine reptiles (e.g. Buffrénil and Mazin, 1990, 1992; Houssaye, 2013; Klein et al., 2015a, 2015b). In modern mammals, marine species also have higher growth rates than terrestrial species (White, 2011). The increased growth rate in *Simosaurus*, however, is still consistent with the variability in rates seen in extant reptiles (Fig. 7B). Growth rates in extant ectothermic animals reflect ambient temperature conditions with tropical species usually having higher rates than temperate species. *Simosaurus* lived in a shallow sea in a warm subtropical climate presumably allowing higher growth rates.

4.4. Life history of Simosaurus

Logistic growth models best described growth in the *Simosaurus* specimens studied (for SMNS 18698 the linear model was similar well supported, Table 2), except for the femur SMNS 18038, in which growth follows the von Bertalanffy model. Nevertheless, both models were applicable to all specimens (Table 2). Both sigmoidal standard models have also been successfully used to describe growth in extant reptiles. Moreover, both models were applicable to two different individuals from a single species (Frazer and Erhart, 1985; Halliday and Verrell, 1988; Magnusson and Sanaiotti, 1995; Ritz et al., 2010). The von Bertalanffy model estimated for SMNS 18038 a hatchling mass of 10.5 ± 1.5 kg. However, this mass is unrealistic high compared to SMNS 18698 (400 g), and could strongly question the biological reliability of this von Bertalanffy model. Alternatively, the high hatchling masses estimated by the growth models for SMNS 18689, but also for SMNS 18038 and SMNS 52095 (Table 2), could indicate ovoviviparity in *Simosaurus* and a large mass of the offspring. The von Bertalanffy growth model predicted for SMNS 18038 that the individual died during its eight year of life, whereas the growth

record suggested that it lived at least one year longer. The logistic models found for SMNS 52095, SMNS 18698, and SMNS 18689 estimated ages at death of individuals between 7 and 13 years, which all agree with the histological record. The observed low longevities in *Simosaurus* specimens could indicate a stronger predation pressure on this taxon than seen in similar-sized extant reptiles. However, longevities are expectancies at the population level that cannot be reliable estimated from few individuals. The predicted asymptotic masses of specimens ranged between 113 and 129 kg, and the derived ages at which asymptotic masses were reached ranged between 10 and 20 years. The estimated ages at which the asymptotic mass is reached are considerably lower than those seen in large extant species (*Alligator mississippiensis*: 150 kg, 73 years in captivity, *Caretta caretta*: 156.5 kg, 37 years, *Chelonia myda*: 160 kg, 75 years, *Varanus komodoensis*: 87 kg, 62 years; data from database AnAge, Tacutu et al., 2013). However, all estimates on asymptotic masses and ages in *Simosaurus* are not well constrained as none of the specimens studied well covers the asymptotic phase of growth. Especially, estimated asymptotic masses of SMNS 18698 and SMNS 18038 have high standard errors (Table 2). An analysis of the growth record of fully-grown individuals could reveal more precise asymptotic masses and ages in *Simosaurus* than the individuals could that were only available for this study. This would also allow to proof whether longevities and asymptotic ages are indeed lower than in extant similar-sized reptiles. The predicted onsets of sexual maturity (location of the inflection point) of specimens were between 3 and 9 years. These estimated ages at the onset of sexual maturity in *Simosaurus* specimens are more or less consistent with those of similar-sized (body mass) extant aquatic and semi-aquatic reptiles (*Alligator mississippiensis*: 150 kg, 12 years; *Caretta caretta*: 156.5 kg, 10 years; *Chelonia mydas*: 160 kg, 10 years; *Varanus komodoensis*: 87 kg, 5 years; data from database AnAge, Tacutu et al., 2013). However, given that asymptotic ages in *Simosaurus* could have been underestimated in the current study they could contrary indicate an earlier maturity in *Simosaurus* than in similar-sized extant reptiles or a sexual dimorphism as was already suggested based on morphology (Rieppel, 1994). The current observations on the life history of *Simosaurus* questions whether extant aquatic and semi-aquatic reptiles are good models for *Simosaurus* and other Sauropterygia (Klein et al., 2015b). It could indicate differing life history strategies in extinct marine reptiles and modern forms. However, this hypothesis has to be tested in the future based on much more samples of *Simosaurus*.

Acknowledgements

We acknowledge Ch. Wimmer-Pfeil (SMNS) for the production of the thin sections. A. Houssaye (CNRS) is thanked for helpful comments on microanatomy and the rerun of the PCA. R. Schoch allowed to sample the bones under his care. M. Sander (StIPB) gave permission to use the technical equipment at the Steinmann Institute, Paleontology, University of Bonn (StIPB). M. Rasser and R. Baumann (both SMNS) provided technical support. We are grateful to the helpful comments of the two reviewers, A. Houssaye (CNRS), J. Both-Brink (NMQR), and the editor M. Laurin.

References

Akaike, H., 1973. Information theory and extension of the maximum likelihood principle. In: Petrov, B.N., Csaki, F. (Eds.), Proceedings of the 2nd International Symposium on Information Theory. Akademiai Kiado, Budapest, pp. 276–281.

Anderson, J.F., Hall-Martin, A., Russell, D.A., 1985. Long bone circumference and weight in mammals, birds, and dinosaurs. J. Zool. S. A 207, 53–61.

Bakker, R.T., 1980. Dinosaur heresy-dinosaur renaissance: why we need endothermic archosaurs for a comprehensive theory of bioenergetic evolution. In: Thomas, D.K., Olson, E.C. (Eds.), A cold look at warm-blooded dinosaurs. American Association for the Advancement of Science, Washington, D.C., pp. 351–362.

Bickelmann, C., Sander, P.M., 2008. A partial skeleton and isolated humeri of *Nothosaurus* (Reptilia: Eosauropterygia) from Winterswijk, The Netherlands. J. Vertebr. Paleontol. 28, 326–338.

Buffrénil de, V., Mazin, J.M., 1990. Bone histology of the ichthyosaurs: comparative data and functional interpretation. Paleobiology 16, 435–447.

Buffrénil de, V., Mazin, J.M., 1992. Contribution de l'histologie osseuse à l'interpretation paléobiologique du genre *Placodus* Agassiz, 1833 (Reptilia, Placodontia). Rev. Paleobiol. 11, 397–407.

Buffrénil de, V., Castanet, J., 2000. Age estimation by skeletochronology in the Nile monitor lizard (*Varanus niloticus*), a highly exploited species. J. Herpetol. 34, 414–424.

Buffrénil de, V., Mazin, J.M., Ricqlès de, A., 1987. Caractères structuraux et mode de croissance du fémur d'*Omphalosaurus nisseri*, ichthyosaurien du Trias moyen de Spitsberg. Ann. Paleontol. 73, 195–216.

Buffrénil de, V., Ricqlès de, A., Ray, C.E., Domning, D.P., 1990. Bone histology of the ribs of the archaeocetes (Mammalia: Cetacea). J. Vertebr. Paleontol. 10 (4), 455–466.

Burnham, K.P., Anderson, D.R., 2002. Model selection and multimodal inference: a practical information-theoretic approach. Springer Press, New York, 488 p.

Campione, N.E., Evans, D.C., 2012. A universal scaling relationship between body mass and proximal limb bone dimensions in quadrupedal terrestrial tetrapods. BMC Biol. 10, 60, http://dx.doi.org/10.1186/1741-7007-10-60.

Canoville, A., Laurin, M., 2010. Evolution of humeral microanatomy and lifestyle in amniotes, and some comments on paleobiological inferences. Biol. J. Linn. Soc. 100 (2), 384–406.

Castanet, J., 1994. Age estimation and longevity in reptiles. Gerontology 40, 174–192.

Castanet, J., Francillon-Vieillot, H., Meunier, F.J., Ricqlès, de, A., 1993. Bone and individual aging. In: Hall, B.K. (Ed.), Bone volume 7: bone growth-B. CRC Press, Boca Raton, Florida, pp. 245–277.

Chen, X.-h., Motani, R., Cheng, L., Jiang, D.Y., Rieppel, O., 2014. The enigmatic marine reptile *Nanchangosaurus* from the Lower Triassic of Hubei, China and the phylogenetic affinities of Hupehsuchia. PLoS ONE 9 (7), e102361, http://dx.doi.org/10.1371/journal.pone.0102361.

Cheng, Y.N., Holmes, R., Wu, X.C., Alfonso, N., 2009. Sexual dimorphism and life history of *Keichousaurus hui* (Reptilia: Sauropterygia). J. Vertebr. Paleontol. 29, 401–408.

Cerda, I.A., Chinsamy, A., 2012. Biological implications of the bone microstructure of the Late Cretaceous Ornithopod Dinosaur *Gasparinisaura cincosaltensis*. J. Vertebr. Paleontol. 32 (2), 355–368.

Chinsamy Turan, A., 2011. Forerunners of mammals – Radiation-Histology-Biology. Indiana University Press, Bloomington, 330 p.

Currey, J.D., 2002. Bones: structure and mechanics. Princeton University Press, Princeton, 456 p.

Dumont, M., Laurin, M., Jacques, F., Pellé, E., Dabin, W., Buffrénil de, V., 2013. Inner architecture of vertebral centra in terrestrial and aquatic mammals: a two dimensional comparative study. J. Morphol. 274 (5), 570–584.

Erickson, G.M., Tumanova, T.A., 2000. Growth curve of *Psittacosaurus mongoliensis* Osborn (Ceratopsia: Psittacosauridae) inferred from long bone histology. Zool. J. Linn. Soc. Lon. 130, 551–566.

Fitzhugh, H.A., 1976. Analysis of growth curves and strategies for altering their shape. J. Anim. Sci. 42, 1036–1051.

Francillon-Vieillot, H., Buffrénil de, V., Castanet, J., Géradudie, J., Meunier, F.J., Sire, J.Y., et al., 1990. Microstructure and mineralization of vertebrate skeletal tissues. In: Carter, J.G. (Ed.), Skeletal biomineralization: patterns, processes and evolutionary trends, Volume 1. Van Norstrand Reinhold, New York, pp. 471–530.

Frazer, N.B., Ehrhart, L.M., 1985. Preliminary growth models for Green, *Chelonia mydas*, and Loggerhead, *Caretta caretta*, turtles in the wild. Copeia 1, 73–79.

Germain, D., Laurin, M., 2005. Microanatomy of the radius and lifestyle in amniotes (Vertebrata, Tetrapoda). Zool. Scripta 34, 335–350.

Girondot, M., Laurin, M., 2003. Bone profiler: a tool to quantify, model and statistically compare bone section compactness profiles. J. Vertebr. Paleontol. 23, 458–461.

Griebeler, E.M., Klein, N., Sander, M.P., 2013. Aging, maturation and growth of sauropodomorph dinosaurs as deduced from growth curves using long bone histological data. PLoS ONE 8 (6), e67012, http://dx.doi.org/10.1371/journal.pone.0067012.

Halliday, T.R., Verrell, P.A., 1988. Body size and age in amphibians and reptiles. J. Herpetol. 22, 253–265.

Hayashi, S., Houssaye, A., Nakajima, Y., Chiba, K., Inuzuka, N., Sawamura, H., Ando, T., Osaki, T., Kaneko, N., 2013. Bone histology suggests increasing aquatic adaptations in Desmostylia (Mammalia, Afrotheria). PLoS ONE. (4), e59146, http://dx.doi.org/10.1371/journal.pone.0059146.

Houssaye, A., 2009. "Pachyostosis" in aquatic amniotes: a review. Integr. Zool. 4, 325–340, http://dx.doi.org/10.1111/j.1749-4877.2009.00146.x (Pmid: 21392306).

Houssaye, A., 2013. Bone histology of aquatic reptiles: what does it tell us about secondary adaptation to an aquatic life? Biol. J. Linn. Soc. 108 (1), 3–21.

Houssaye, A., Scheyer, T.M., Kolb, C., Fischer, V., Sander, P.M., 2014. A new look at ichthyosaur long bone microanatomy and histology: implications for their adaptation to an aquatic life. PLoS ONE 9 (4), e95637, http://dx.doi.org/10.1371/journal.pone.0095637.

Houssaye, A., Lindgren, J., Pellegrini, R., Lee, A.H., Germain, D., et al., 2013. Microanatomical and histological features in the long bones of Mosasaurine Mosasaurs (Reptilia, Squamata) – implications for aquatic adaptation and growth rates. PLoS ONE 8 (10), e76741, http://dx.doi.org/10.1371/journal.pone.0076741.

Houssaye, A., Mazurier, A., Herrel, A., Volpato, V., Tafforeau, P., Boistel, R., Buffrénil de, V., 2010. Vertebral microanatomy in squamates: structure, growth and ecological correlates. J. Anat. 217, 715–727.

Hugi, J., 2011. The long bone histology of *Ceresiosaurus* (Sauropterygia, Reptilia) in comparison to other eosauropterygians from the Middle Triassic of Monte San Giorgio (Switzerland/Italy). Swiss J. Palaeontol, http://dx.doi.org/10.1007/s13358-011-0023-6.

Hugi, J., Sánchez-Villagra, M.R., 2012. Histological and skeletochronological analyses on life history and skeletal adaptations in the marine iguana *Amblyrhynchus cristatus* and in other iguanas. J. Herpetol. 46, 312–324.

Hugi, J., Scheyer, T.M., Sander, P.M., Klein, N., Sánchez-Villagra, M.R., 2011. Long bone microstructure gives new insights into the life history data of pachypleurosaurids from the Middle Triassic of Monte San Giorgio, Switzerland/Italy. C. R. Palevol. 10, 413–426.

Klein, N., 2010. Long bone histology of Sauropterygia from the Lower Muschelkalk of the Germanic basin provides unexpected implications for phylogeny. PLoS ONE 5, e11613, http://dx.doi.org/10.1371/journal.pone.0011613.

Klein, N., 2012. Postcranial morphology and growth of the Winterswijk pachypleurosaur *Anarosaurus heterodontus* (Sauropterygia) from the Lower Muschelkalk of Winterswijk, The Netherlands. Pal. Z. 86 (4), 389–408.

Klein, N., Sander, P.M., 2007. Bone histology and growth of the prosauropod *Plateosaurus engelhardti* Meyer, 1837 from the Norian bonebeds of Trossingen (Germany) and Frick (Switzerland). Spec. Pap. Palaeontol. 77, 169–206.

Klein, N., Houssaye, A., Neenan, J.M., Scheyer, T.M., 2015a. Long bone histology and microanatomy of Placodontia (Diapsida: Sauropterygia). Contrib. Zool. 89, 59–84.

Klein, N., Neenan, J., Scheyer, T.M., Griebeler, E.M., 2015b. Growth patterns and life history strategies in Placodontia (Diapsida: Sauroptertygia). R. Soc. Open Sci. 2, 140440, http://dx.doi.org/10.1098/rsos.140440.

Klein, N., Sander, M.P., Stein, K., Le Loeuff, J., Carballido, J., Buffetaut, E., 2012a. Modified laminar bone in *Ampelosaurus atacis* and other titanosaurs (Sauropoda): Implications for life history and physiology. PLoS ONE 7 (5), e36907, http://dx.doi.org/10.1371/journal.pone.0036907.

Klein, N., Christian, A., Sander, P.M., 2012b. Histology shows that elongated neck ribs in sauropod dinosaurs are ossified tendons. Biol. Lett., http://dx.doi.org/10.1098/rsbl.2012.0778.

Köhler, M., Marín-Moratalla, N., Jordana, X., Aanes, R., 2012. Seasonal bone growth and physiology in endotherms shed light on dinosaur physiology. Nature 487, 358–361.

Konietzko-Meier, D., Klein, N., 2013. Unique growth pattern of *Metoposaurus diagnosticus krasiejowensis* (Amphibia, Temnospondyli) from the Upper Triassic of Krasiejow, Poland. Palaeogeogr., Palaeoclimatol., Palaeoecol. 370, 145–157.

Konietzko-Meier, D., Schmitt, A., 2013. A histological study of a femur of *Plagiosuchus*, a Middle Triassic temnospondyl amphibian from southern Germany, using thin sections and micro-CT scanning. In: Mulder, E.W.A., Jagt, J.W.M., Schulp, A.S. (Eds.), The Sunday's child of Dutch earth sciences - a tribute to Bert Boekschoten on the occasion of his 80th birthday. Geosci J. 92 (2–3), 97–108.

Krahl, A., Klein, N., Sander, P.M., 2013. Evolutionary implications of the divergent long bone histologies of *Nothosaurus* and *Pistosaurus* (Sauropterygia, Triassic). BMC Evol. Biol. 13, 1–23.

Kupfer, A., Kramer, A., Himstedt, W., 2004. Sex-related growth patterns in a caecilian amphibian (genus *Ichthyophis*): evidence from laboratory data. J. Zool., Lond. 262, 173–178.

Laurin, M., Girondot, M., Loth, M.M., 2004. The evolution of long bone microanatomy and lifestyle in lissamphibians. Paleobiolology 30, 589–613.

Laurin, M., Meunier, F.J., Germain, D., Lemoine, M., 2007. A microanatomical and histological study of the paired fin skeleton of the Devonian sarcopterygian *Eusthenopteron foordi*. J. Paleontol. 81 (1), 143–153.

Laurin, M., Canoville, A., Germain, D., 2011. Bone microanatomy and lifestyle: a descriptive approach. C. R. Palevol 10, 381–402.

Lee, A.H., Werning, S., 2008. Sexual maturity in growing dinosaurs does not fit reptilian growth models. Proc. Natl. Acad. Sci. USA 105, 582–587.

Lin, K., Rieppel, O., 1998. Functional morphology and ontogeny of *Keichousaurus hui* (Reptilia, Sauropterygia). Fieldiana (Geology), n.s. 39, 1–35.

Magnusson, W.E., Sanaiotti, T.M., 1995. Growth of *Caiman crocodilus* in central Amazonia, Brazil. Copeia 2, 498–501.

Margerie, D.E., Robin, J.P., Verrier, D., Cubo, J., Groscolas, R., Castanet, J., 2004. Assessing a relationship between bone microstructure and growth rate: a fluorescent labelling study in the king penguin chick (*Aptenodytes patagonicus*). J. Exp. Biol. 207, 869–879.

Meyer, V.H., 1842. *Simosaurus*, die Stumpfschnauze, ein Saurier aus dem Muschelkalke von Luneville. N. Jb. Mineral., Geogn., Geol. Petrefktk 1842, 184–197.

Montes, L., Le Roy, N., Perret, M., Buffrénil de, V., Castanet, J., Cubo, J., 2007. Relationships between bone growth rate, body mass and resting metabolic rate in growing amniotes: a phylogenetic approach. Biol. J. Linn. Soc. 92, 63–76.

Nakajima, Y., Hirayama, R., Endo, H., 2014. Turtle humeral microanatomy and its relationship to lifestyle. Biol. J. Linn. Soc. 112, 719–734.

Neenan, J.M., Klein, N., Scheyer, T.M., 2013. European origin of placodont marine reptiles and the evolution of crushing dentition in Placodontia. Nat. Comm. 4 (1621), 1–7, http://dx.doi.org/10.1038/ncomms2633.

Padian, K., Horner, J.R., 2004. Dinosaur physiology. In: Weishampel, D.B., Dodson, P., Osmólska, H. (Eds.), The Dinosauria. , 2nd Edition. University of California Press, Berkeley, pp. 660–671.

Padian, K., Horner, J.R., Ricqlès de, A., 2004. Growth in small dinosaurs and pterosaurs: the evolution of archosaurian growth strategies. J. Vertebr. Paleontol. 24 (3), 555–571.

Quemeneur, S., Buffrénil de, V., Laurin, M., 2013. Microanatomy of the amniote femur and inference of lifestyle in limbed vertebrates. Biol. J. Linn. Soc. 109 (3), 644–655.

Quinn, G.P., Keough, M.J., 2002. Experimental design and data analysis for biologists. Cambridge University Press, Cambridge, 537 p.

Reiss, M.J., 1989. The allometry of growth and reproduction. Cambridge University Press, New York, 200 p.

Richards, F.J., 1959. A flexible growth function for empirical use. J. Exp. Bot. 10, 290–300.

Ricqlès de, A., 1983. Cyclical growth in the long limb bones of a sauropod dinosaur. Acta Palaeontol. Pol. 28, 225–232.

Ricqlès de, A., 1976. On bone histology of fossil and living reptiles, with comments on its functional and evolutionary significance. In: Bellairs, A.D.A, Cox, C.B. (Eds.), Linnean Society Symposium Series No. 3. Morphology and biology of reptiles. Academic Press, London, pp. 123–150.

Ricqlès de, A., 1992. Paleoherpetology now: a point of view. In: Adler, K. (Ed.), Herpetology: current research on the biology of amphibians and reptiles. Proceedings of the First World Herpetological Congress. Society for the Study of Amphibians and Reptiles, Oxford, pp. 1197–1200.

Ricqlès de, A., Buffrénil de, V., 2001. Bone histology, heterochronies and the return of tetrapods to life in water: where are we? In: Mazin, J.M., Buffrénil de, V. (Eds.), Secondary adaptation of tetrapods to life in water. Friedrich Pfeil Verlag, Munich, Germany, pp. 289–310.

Ricqlès de, A., Padian, K., Horner, J.A., 2003. On the bone histology of some Triassic pseudosuchian archosaurs and related taxa. Ann. Paleontol. 89 (2), 67–101.
Rieppel, O., 1994. Osteology of *Simosaurus gaillardoti*, and the phylogenetic interrelationships of stem-group Sauropterygia. Fieldiana (Geology), n.s. 28, 1–85.
Rieppel, O., 2000. Sauropterygia I. In: Wellnhofer, P. (Ed.), Encyclopedia of Paleoherpetology, Volume 12A. Friedrich Pfeil Verlag, München, pp. 1–134.
Ritz, J., Griebeler, E.M., Huber, R., Clauss, M., 2010. Body size development of captive and free ranging African spurred tortoises (*Geochelone sulcata*): high plasticity in reptilian growth rates. Herp. J. 20, 213–216.
Sander, P.M., 1989. The pachypleurosaurids (Reptilia: Nothosauria) from the Middle Triassic of Monte San Giorgio (Switzerland), with the description of a new species. Phil. Trans. Royal Soc. London B 325, 561–670.
Sander, P.M., 1990. Skeletochronology in the small Triassic reptile *Neustikosaurus*. Ann. Sci. Nat., Zool. 13 (11), 213–217.
Sander, P.M., Klein, N., 2005. Developmental plasticity in the life history of a prosauropod dinosaur. Science 310, 1800–1802.
Sanchez, S., Schoch, R.R., Ricqlès de, A., Steyer, J.S., 2010. Palaeoecological and palaeoenvironmental influences revealed by long-bone palaeohistology: the example of the Permian branchiosaurid Apateon. In: Vecoli, M., Clément, G., Meyer, B. (Eds.), The terrestrialization process: modelling complex interactions at the biosphere geosphere interface. The Geological Society, London, pp. 137–147.
Tacutu, R., Craig, T., Budovsky, A., Wuttke, D., Lehmann, G., Taranukha, D., Costa, J., Fraifeld, V.E., de Magalhaes, J.P., 2013. Human ageing genomic resources: integrated databases and tools for the biology and genetics of ageing. Nucleic Acids Research 41 (D1), D1027–D1033.
Werner, J., Griebeler, E.M., 2014. Allometries of maximum growth rate versus body mass at maximum growth indicate that non-avian dinosaurs had growth rates typical of fast growing ectothermic sauropsids. PLoS ONE 9 (2), e88834, http://dx.doi.org/10.1371/journal.pone.0088834.
Wiffen, J., Buffrénil de, V., Ricqlès de, A., Mazin, J.M., 1995. Ontogenetic evolution of bone structure in Late Cretaceous Plesiosauria from New Zealand. Geobios 28, 625–640.
Witzmann, F., 2009. Comparative histology of sculptured dermal bones in basal tetrapods, and the implications for the soft tissue dermis. Palaeodiversity 2, 233–270.
White, C.R., 2011. Allometric estimation of metabolic rates in animals. Comp. Biochem. Phys., Part A 158, 346–357, http://dx.doi.org/10.1016/j.cbpa.2010.10.004.